

UNO: Unlimited Sampling Meets One-Bit Quantization

Arian Eamaz, *Graduate Student Member, IEEE*, Kumar Vijay Mishra, *Senior Member, IEEE*, Farhang Yeganegi, and Mojtaba Soltanalian, *Senior Member, IEEE*

Abstract

Recent results in one-bit sampling provide a framework for a relatively low-cost, low-power sampling, at a high rate by employing time-varying sampling threshold sequences. Another recent development in sampling theory is unlimited sampling, which is a high-resolution technique that relies on *self-reset ADCs* to yield an unlimited dynamic range. In this paper, we leverage the appealing attributes of the two aforementioned techniques to propose a novel *unlimited one-bit (UNO)* sampling approach. In this framework, the information on the distance between the input signal value and the threshold are stored and utilized to accurately reconstruct the one-bit sampled signal. We then utilize this information to accurately reconstruct the signal from its one-bit samples via the randomized Kaczmarz algorithm (RKA); a strong linear feasibility solver that selects a random linear equation at each iteration. In the presence of noise, we employ the recent plug-and-play (PnP) priors technique with alternating direction method of multipliers (ADMM) to exploit integration of state-of-the-art regularizers in the reconstruction process. Numerical experiments with RKA and PnP-ADMM-based reconstruction illustrate the effectiveness of our proposed UNO, including its superior performance compared to the one-bit $\Sigma\Delta$ sampling.

Index Terms

Kaczmarz algorithm, one-bit quantization, PnP-ADMM, self-reset ADCs, unlimited sampling.

This work was supported in part by the National Science Foundation Grant CCF-1704401. The conference precursor to this work has been submitted for publication at the 2023 IEEE International Conference on Acoustics, Speech and Signal Processing (ICASSP)

(Corresponding author: Arian Eamaz)

A. Eamaz, F. Yeganegi, and M. Soltanalian are with the Department of Electrical and Computer Engineering, University of Illinois Chicago, Chicago, IL 60607, USA (e-mail: {*aeamaz2*, *fyegan2*, *msol*}@*uic.edu*).

K. V. Mishra is with the United States DEVCOM Army Research Laboratory, Adelphi, MD 20783 USA (e-mail: *kvm@ieee.org*).

I. INTRODUCTION

Sampling theory lies at the heart of all modern digital processing systems. The original sampling problem entails identifying a continuous function on Euclidean space from discrete data samples. It is addressed by the classical sampling theorem, commonly and variously, attributed to Cauchy [1], de La Vallée Poussin [2], Whittaker [3], Ogura [4], Kotelnikov [5], Raabe [6], Shannon [7], and/or Someya [8]. A seminal result in this context, referred to as Whittaker-Kotelnikov-Shannon (or, simply Shannon's) theorem, states that it is possible to fully recover a bandlimited function from values measured on a regular sampling grid as long as the bandlimitation is an interval with length not exceeding the density of the sampling grid. Restating this in signal processing terms, a lowpass bandlimited signal can be perfectly reconstructed from its discrete samples taken uniformly at a sampling frequency that is at least the Nyquist rate, i.e., twice the signal bandwidth. During the past few decades, several variants and extensions of this result have solidified the extensive role of sampling theory in science and engineering [9–11].

Shannon's theorem assumes the existence of samples that are of infinite precision and infinite dynamic range (DR). But, in practice, it is realized by the quantization of the signals through analog-to-digital converters (ADCs) that clip or saturate whenever the signal amplitude exceeds the maximum recordable ADC voltage, leading to a significant information loss. The effects of finite precision quantization are characterized in the form of rate distortion theory [12, 13]. However, investigations into finite DR or clipping effects are relatively recent [14–17]. Substantial work has been done and is still ongoing to overcome this problem, and the literature is too large to summarize here; see, e.g., [18] and the references therein, for comparisons of various techniques. Overall, these approaches require declipping [19], multiple ADCs [20], and scaling techniques [21], which are expensive and cumbersome. Recently, some studies [18, 22, 23] have proposed the *unlimited sampling* architecture to fully overcome this limitation by employing modular arithmetic. To perfectly reconstruct the signal of interest from modulo samples (up to a unknown constant), the unlimited sampling theory suggests the sampling rate to be slightly higher than the Nyquist rate and the norm estimate of the bandlimited signal be known.

Conventional multi-bit ADCs require a very large number of quantization levels to represent the original continuous signal in high resolution settings. Sampling at high data rates with high resolution ADCs, however, would dramatically increase the overall power consumption and the manufacturing cost of such ADCs [24]. This problem is exacerbated in systems that require multiple ADCs such as large array receivers [25]. An immediate solution to such challenges is to use fewer bits for sampling. Therefore, in the recent years, the design of receivers with low-complexity *one-bit ADC* has been emphasized to meet

the requirements of both wide signal bandwidth and low cost/power. *One-bit quantization* is an extreme quantization scenario, in which the ADCs are merely comparing the signals with given threshold levels, producing sign (± 1) outputs. This enables the signal processing equipment to sample at a very high rate yet with considerably lower cost and energy consumption than the conventional ADCs [24, 26–29].

In the classical problem of one-bit sampling, the signal is reconstructed by comparing the signal with a fixed, usually zero, threshold. This leads to difficulties in estimating signal parameters. In particular, when zero threshold is used, the power information of the input signal \mathbf{x} is lost in one-bit data because the signs of \mathbf{x} and $\eta\mathbf{x}$ are identical for $\eta > 0$. This problem has been addressed in a few recent works [28, 30–35], which show that time-varying sampling thresholds enable better estimation of the signal characteristics. In particular, time-varying thresholds were considered for the covariance recovery from one-bit measurements in [28]. This was extended in [33] for a significantly improved estimation of signal autocorrelation via the *modified arcsine law*. In non-stationary scenarios, [33] applied the modified arcsine law to utilize time-varying sampling thresholds. Applications of one-bit sampling to diverse problems such as sparse parameter estimation [31], localization [36], and phase retrieval [32] have also appeared in the contemporary literature.

Evidently, one-bit and unlimited sampling frameworks address complementary requirements. A one-bit ADC only compares an input signal with a given threshold. Therefore, essentially, one-bit sampling is indifferent to DR because, apart from the comparison bit, other information such as the distance between the signal value and the threshold is not stored. On the other hand, the self-reset ADC in unlimited sampling provides a natural approach to producing judicious time-varying thresholds for one-bit ADCs. In this paper, to harness advantages of both methods, we propose *unlimited one-bit* (UNO) sampling to design sampling thresholds which are highly informative about the signal of interest.

A. Prior Art

Unlimited sampling of continuous-time signals that are sparse in Fourier domain was discussed in [37]. Extensions to graph signals [38], multi-channel arrays [39], and sparse outliers (noise) [40] have also been proposed. Reconstruction algorithms have included wavelet-based [23], generalized approximate message passing [41], and local average [42] techniques. Very recently, non-idealities in hardware prototyping were considered in [43, 44]; a computational sampling strategy in the form of *unlimited sampling with hysteresis* [45] was found to be more flexible for circuit design specifications.

To reconstruct the full-precision signal from one-bit sampled data, conventional approaches [46, 47] include maximum likelihood estimation (MLE) and weighted least squares. However, these methods have high computational cost, especially for high-dimensional input signals. To this end, we propose using the

randomized Kaczmarz algorithm (RKA) [48, 49], which is an iterative algorithm for solving a system of linear inequalities that arise naturally in the one-bit quantization framework. While the deterministic version [50] of the Kaczmarz method usually selects the linear equation sequentially, the RKA is random in its selection in each iteration leading to a faster convergence. The RKA is simple to implement and performs comparably with the state-of-the-art optimization methods.

Among prior studies involving both one-bit and unlimited frameworks, state-of-the-art results in [51] proposed *one-bit $\Sigma\Delta$ quantization via unlimited sampling*, whose objective is to shrink the *DR between the input signal and its one-bit samples*. This study developed a guaranteed reconstruction as long as the DR of the input signal is less than the DR of the one-bit data (i.e., 1). However, when the ratio of the input signal amplitude to the ADC threshold is large, then the imperfect noise shaping in sigma-delta conversion degrades this reconstruction. Contrary to this work, our proposed UNO technique focuses on a different problem, i.e., shrinking the *DR between the input signal and the time-varying sampling thresholds*. The one-bit sampling is typically performed at significantly high rates. As a result, the resulting observation inequalities form an overdetermined system. When the difference between the DR of the input signal and that of the thresholds increases, the reconstruction degrades significantly. We show that jointly exploiting both unlimited and one-bit sampling techniques provides a more efficient solution by a considerable reduction of the aforementioned gap.

In practice, errors arising from quantization noise degrade the reconstruction quality in unlimited sampling framework. In this context, [18] derived the reconstruction guarantees by including this error as bounded additive noise to the modulo samples. Contrary to this approach, we consider the more realistic case of additive noise to the input signal. We show that our RKA-based reconstruction is also effective for noisy one-bit sampled signals because it is independent from the statistical properties of the modulo samples.

B. Our Contributions

Our main contributions in this paper are:

1) Combined unlimited and one-bit sampling framework. In the proposed UNO framework, we leverage upon the benefits of both one-bit and unlimited sampling techniques. The result is a sampling approach that yields unlimited DR and a low-cost, low-power receiver while retaining a high sampling rate. We design time-varying sampling thresholds for one-bit quantization, whose DR is closer to that of the original signal. This aids in accurately storing the information of distance between the signal values and thresholds to utilize in the signal reconstruction task. We show that compared to the one-bit reconstruction with random thresholds [24], our proposed UNO sampling based on time-varying

thresholds performs better, especially for high DR signals.

2) RKA-based reconstruction. The signal reconstruction from one-bit measurements requires solving an overdetermined linear feasibility problem that we recast as a one-bit polyhedron and efficiently solve it via the RKA. By generating an abundant number of one-bit samples, we show that the singular values of one-bit data matrix that creates the one-bit polyhedron are equal to the number of time-varying threshold sequences employed in one-bit sampling. Further, we numerically investigate the effects of ADC threshold and signal amplitude in the RKA-based UNO reconstruction.

3) Performance guarantees. Our theoretical analyses show that a proper selection of the sufficient number of samples further enhances the reconstruction performance of the UNO. We prove that the convergence rate of the RKA when applied to the one-bit polyhedron depends on the size of the input signal and the total number of RKA iterations. In this context, we also obtain a lower bound on the number of required iterations for perfect reconstruction.

4) Reconstruction in the presence of additive noise. When the input signal is contaminated with additive noise, we apply the recently introduced new plug-and-play (PnP) priors [52] to the alternating direction method of multipliers (ADMM) as an additional reconstruction algorithm step. In image denoising problems, the PnP-ADMM is used to replace the shrinkage step of the standard ADMM algorithm with any off-the-shelf algorithm to ensure the noise variance is sufficiently suppressed. Although PnP-ADMM appears *ad hoc*, it yields a better performance than state-of-the-art methods in several different inverse problems [52, 53]. For the noisy UNO, we deploy this algorithm to reconstruct the original signal from overdetermined and underdetermined noisy systems. Moreover, we show that the additive noise to the input signal contaminates the modulo samples with noise that is expressed in terms of the input noise.

C. Organization and Notations

In the next section, we provide an introduction to one-bit quantization with time-varying sampling thresholds. Particularly, the one-bit sampled signal reconstruction problem is formulated as an overdetermined system of linear inequalities. In Section III, we recall the concept of unlimited sampling as proposed in [18, 22]. We introduce the RKA in the context of signal reconstruction in Section IV. This is a prelude to Section V, which proposes UNO sampling to design judicious thresholds and guarantee the one-bit signal reconstruction in the high-DR. In Section VI, we provide several numerical experiments to illustrate UNO-based sampling and analyze the reconstruction error. We consider the noisy measurement scenario in Section VII and conclude in Section VIII.

Throughout this paper, we use boldface lowercase, boldface uppercase, and calligraphic letters for vectors, matrices, and sets, respectively. The notations \mathbb{C} , \mathbb{R} , and \mathbb{Z} represent the set of complex, real, and

integer numbers, respectively. We represent a vector \mathbf{x} in terms of its elements $\{x_i\}$ or $(\mathbf{x})_i$ as $\mathbf{x} = [x_i]$. We use $(\cdot)^\top$ and $(\cdot)^H$ to denote the vector/matrix transpose and the Hermitian transpose, respectively. The identity matrix of size N is $\mathbf{I}_N \in \mathbb{R}^{N \times N}$. The Frobenius norm of a matrix $\mathbf{B} \in \mathbb{C}^{M \times N}$ is defined as $\|\mathbf{B}\|_F = \sqrt{\sum_{r=1}^M \sum_{s=1}^N |b_{rs}|^2}$, where b_{rs} is the (r, s) -th entry of \mathbf{B} . The function $\text{diag}(\cdot)$ outputs a diagonal matrix with the input vector along its main diagonal. The ℓ_p -norm of a vector \mathbf{b} is $\|\mathbf{b}\|_p = (\sum_i b_i^p)^{1/p}$. The infinity or max-norm of a function x is $\|x\|_\infty = \inf \{c_0 \geq 0 : |x(t)| \leq c_0\}$, where $\inf(\cdot)$ denotes the infimum of its argument; for vectors, we have $\|\mathbf{x}\|_\infty = \max_k |x_k|$. For a vector \mathbf{x} , $\Delta \mathbf{x} = x_{k+1} - x_k$ denotes the finite difference and recursively applying the same yields N -th order difference, $\Delta^N \mathbf{x}$. We denote the Ω -bandlimited Paley-Wiener subspace of the square-integrable function space L^2 by PW_Ω such that $\text{PW}_\Omega = \{f : f, \hat{f} \in L^2, \text{supp}(\hat{f}) \subset [-\Omega, \Omega]\}$, where \hat{f} is the Fourier transform of f . The Hadamard (element-wise) product of two matrices \mathbf{B}_1 and \mathbf{B}_2 is $\mathbf{B}_1 \odot \mathbf{B}_2$. The column-wise vectorized form of a matrix \mathbf{B} is $\text{vec}(\mathbf{B})$. Given a scalar x , we define the operator $(x)^+$ as $\max\{x, 0\}$. For an event \mathcal{E} , $\mathbb{1}_{(\mathcal{E})}$ is the indicator function for that event meaning that $\mathbb{1}_{(\mathcal{E})}$ is 1 if \mathcal{E} occurs; otherwise, it is zero. The function $\text{sgn}(\cdot)$ yields the sign of its argument. In the context of numerical computations, $\lfloor \cdot \rfloor$ and $\lceil \cdot \rceil$ denote the floor and ceiling functions, respectively. The function $\log(\cdot)$ denotes the natural logarithm, unless its base is otherwise stated. The notation $x \sim \mathcal{U}(a, b)$ means a random variable drawn from the uniform distribution over the interval $[a, b]$ and $x \sim \mathcal{N}(\mu, \sigma^2)$ represents the normal distribution with mean μ and variance σ^2 . The operator $\text{mod}(a, b)$ between two values a and b , returns the remainder of the division operation a/b .

II. ONE-BIT SAMPLING: OVERDETERMINED LINEAR SYSTEM FORMULATION

Several approaches have been proposed in the literature to reconstruct the signal of interest from one-bit samples with the most of them formulating this task as an optimization problem. For example, the covariance matrix formulation of [24] employs the cyclic optimization method to recover the input autocorrelation elements. A convex program based on the Gauss-Legendre integration to recover the input covariance matrix from one-bit sampled data was suggested in [33]. Other recent works exploit sparsity of the signal and apply techniques such as ℓ_1 -norm minimization [54, 55], ℓ_1 -regularized MLE formulation [47, 56], log-relaxation [57], and Lasserre's semidefinite program relaxation [36] to lay the ground for signal reconstruction. In the following, we explain our one-bit polyhedron formulation, wherein a strong efficient and easily implementable solver of linear feasibility problems is applied to the aforementioned application-specific methods.

A. One-Bit Quantization Using Time-Varying Thresholds

Consider a bandlimited continuous-time signal $x \in \text{PW}_\Omega$ that we represent via Shannon's sampling theorem as [10]

$$0 < T \leq \frac{\pi}{\Omega}, \quad x(t) = \sum_{k=-\infty}^{k=+\infty} x(kT) \text{sinc}\left(\frac{t}{T} - k\right), \quad (1)$$

where $1/T$ is the sampling rate, Ω is the signal bandwidth, and $\text{sinc}(t) = \frac{\sin(\pi t)}{\pi t}$ is an *ideal* low-pass filter. Denote the uniform samples of $x(t)$ with the sampling rate $1/T$ by $x_k = x(kT)$.

In practice, the discrete-time samples occupy pre-determined quantized values. We denote the quantization operation on $x[k]$ by the function $Q(\cdot)$. This yields the quantized signal as $r_k = Q(x_k)$. In one-bit quantization, compared to zero or constant thresholds, time-varying sampling thresholds yield a better reconstruction performance [24, 33]. These thresholds may be chosen from any distribution. In this work, to be consistent with state-of-the-art [24, 28, 46], we consider a Gaussian non-zero time-varying threshold vector $\boldsymbol{\tau} = [\tau_k]$ that follows the distribution $\boldsymbol{\tau} \sim \mathcal{N}(\mathbf{d} = \mathbf{1}d, \boldsymbol{\Sigma})$. For one-bit quantization with such time-varying sampling thresholds, $r_k = \text{sgn}(x_k - \tau_k)$.

B. One-Bit Polyhedron

The information gathered through the one-bit sampling with time-varying thresholds may be formulated in terms of an overdetermined linear system of inequalities. We have $r_k = +1$ when $x_k > \tau_k$ and $r_k = -1$ when $x_k < \tau_k$. Collecting all the elements in the vectors as $\mathbf{x} = [x_k] \in \mathbb{R}^n$ and $\mathbf{r} = [r_k] \in \mathbb{R}^n$, therefore, one can formulate the geometric location of the signal as

$$r_k (x_k - \tau_k) \geq 0. \quad (2)$$

Then, the vectorized representation of (2) is $\mathbf{r} \odot (\mathbf{x} - \boldsymbol{\tau}) \geq \mathbf{0}$ or equivalently

$$\boldsymbol{\Omega} \mathbf{x} \succeq \mathbf{r} \odot \boldsymbol{\tau}, \quad (3)$$

where $\boldsymbol{\Omega} \triangleq \text{diag}(\mathbf{r})$. Suppose $\mathbf{x}, \boldsymbol{\tau} \in \mathbb{R}^n$, and that $\boldsymbol{\tau}^{(\ell)}$ denotes the time-varying sampling threshold in ℓ -th signal sequence, where $\ell \in \mathcal{L} = \{1, \dots, m\}$.

For the ℓ -th signal sequence, (3) becomes

$$\boldsymbol{\Omega}^{(\ell)} \mathbf{x} \succeq \mathbf{r}^{(\ell)} \odot \boldsymbol{\tau}^{(\ell)}, \quad \ell \in \mathcal{L}, \quad (4)$$

where $\boldsymbol{\Omega}^{(\ell)} = \text{diag}(\mathbf{r}^{(\ell)})$. Denote the concatenation of all m sign matrices as

$$\tilde{\boldsymbol{\Omega}} = \left[\boldsymbol{\Omega}^{(1)} \mid \dots \mid \boldsymbol{\Omega}^{(m)} \right]^T, \quad \in \mathbb{R}^{mn \times n}. \quad (5)$$

Rewrite the m linear system of inequalities in (4) as

$$\tilde{\Omega}\mathbf{x} \succeq \text{vec}(\mathbf{R}) \odot \text{vec}(\mathbf{\Gamma}), \quad (6)$$

where \mathbf{R} and $\mathbf{\Gamma}$ are matrices, whose columns are the sequences $\{\mathbf{r}^{(\ell)}\}_{\ell=1}^m$ and $\{\boldsymbol{\tau}^{(\ell)}\}_{\ell=1}^m$, respectively.

The linear system of inequalities in (6) associated with the one-bit sampling scheme is overdetermined. We recast (6) into a *one-bit polyhedron* as

$$\mathcal{P} = \left\{ \mathbf{x} \mid \tilde{\Omega}\mathbf{x} \succeq \text{vec}(\mathbf{R}) \odot \text{vec}(\mathbf{\Gamma}) \right\}. \quad (7)$$

Instead of complex high-dimensional optimization with techniques such as MLE, our objective is to employ the polyhedron (7) that encapsulates the desired signal \mathbf{x} and leads to solving linear inequalities with linear convergence in expectation.

III. UNLIMITED SAMPLING

In a variety of applications, clipping or saturation poses a serious problem to signal reconstruction. For instance, in scientific imaging systems such as ultrasound [14], radar [58], and seismic imaging [59], strong reflections or pulse echoes blind the sensor. In audio processing, clipped sound results in high-frequency artifacts [15]. In this context, unlimited sampling suggests that, instead of point-wise samples of the bandlimited function $x(t)$, the signal is digitized using a self-reset ADC with an appropriately selected threshold $\lambda > 0$ such that any signal value outside the range $[-\lambda, \lambda]$ is *folded* to the same range [18, 22]. The folding corresponds to introducing a non-linearity in the sensing process [18, 22]. We denote the folding by the modulo operator \mathcal{M}_λ that represents the following mapping:

$$\mathcal{M}_\lambda(x_k) : \tilde{x}_k = x_k - 2\lambda \left\lfloor \frac{x_k}{2\lambda} + \frac{1}{2} \right\rfloor, \quad (8)$$

where \tilde{x}_k are the modulo samples of $x(t)$.

The *unlimited sampling theorem* [18] (reproduced below) states that, if the estimate of the norm of the bandlimited signal is known, then its perfect reconstruction (up to additive multiples of 2λ) from its modulo samples is possible with at least sampling period $T \leq (2\pi e)^{-1}$, where e is the Euler's number and the signal bandwidth has been normalized to π .

Theorem 1 (Unlimited sampling theorem [18]). *Assume $x(t)$ to be a finite energy, bandlimited signal with maximum frequency Ω_{\max} and let \tilde{x}_k , $k \in \mathbb{Z}$ in (8) be the modulo samples of $x(t)$ with sampling rate $1/T$. Then a sufficient condition for the reconstruction of $x(t)$ from $\{\tilde{x}_k\}$ is that $T \leq \frac{1}{2\Omega_{\max}e}$ (up to additive multiples of 2λ).*

Theorem 1 implies that the sampling rate depends on only the bandwidth and is independent of the ratio of ADC threshold λ to the signal amplitude. In other words, the DR of the input signal is *unlimited*. Recently, stable unlimited sampling reconstruction in the presence of noise has also been obtained [18].

The reconstruction of the bandlimited function $x(t)$ from its modulo samples $\{\tilde{x}_k\}$ is achieved as follows. Assume that $x(t)$ admits a decomposition [18, 22],

$$x(t) = \tilde{x}(t) + \epsilon_x(t), \quad (9)$$

where $\tilde{x}(t) = \mathcal{M}_\lambda(x(t))$ and the error ϵ_x between the input signal and its modulo samples is

$$\epsilon_x(t) = 2\lambda \sum_{u \in \mathbb{Z}} e_u \mathbb{1}_{\mathcal{D}_u}(t), \quad e_u \in \mathbb{Z}, \quad (10)$$

where $\bigcup_{u \in \mathbb{Z}} \mathcal{D}_u = \mathbb{R}$ is a partition of the real line into intervals \mathcal{D}_u . As indicated by (9), if ϵ_x is known, then x can be reconstructed from \tilde{x} . It follows from (10) that ϵ_x takes only those values that are integer multiples of 2λ thereby leading to a robust reconstruction algorithm [18]. To obtain ϵ_x (up to an unknown additive constant) and subsequently the desired signal $x(t)$, the reconstruction procedure in [18, 22] requires the higher-order differences of $\tilde{\mathbf{x}} = [\tilde{x}_k]$ to obtain $\Delta^N \epsilon_x = \mathcal{M}_\lambda(\Delta^N \tilde{\mathbf{x}}) - \Delta^N \tilde{\mathbf{x}}$, where $\epsilon_x = [\epsilon_x]$. Define the inverse-difference operator as a sum of real sequence $\{s_b\}$, i.e.,

$$\nabla : \{s_k\}_{k \in \mathbb{Z}^+} \rightarrow \sum_{b=1}^k s_b. \quad (11)$$

Then, applying $\nabla(\Delta^N \epsilon_x)$ and rounding the result to the nearest multiple of $2\lambda\mathbb{Z}$ yields ϵ_x . For a guaranteed and stable reconstruction performance, a suitable choice for difference order N is [18],

$$N \geq \left\lceil \frac{\log \lambda - \log \beta_x}{\log(T\Omega e)} \right\rceil, \quad (12)$$

where β_x is chosen such that $\beta_x \in 2\lambda\mathbb{Z}$ and $\|x\|_\infty \leq \beta_x$. Algorithm 1 summarizes the unlimited sampling reconstruction procedure.

Algorithm 1 Input signal reconstruction from modulo folded samples.

Input: $\tilde{x}_k = \mathcal{M}_\lambda(x_k)$, ADC threshold λ , and $2\lambda\mathbb{Z} \ni \beta_x \geq \|x\|_\infty$.

Output: The approximation of the input signal $\bar{\mathbf{x}}$.

- 1: $N \leftarrow \left\lceil \frac{\log \lambda - \log \beta_x}{\log(T\Omega e)} \right\rceil$ using (12).
- 2: $\Delta^N \boldsymbol{\epsilon}_x \leftarrow \mathcal{M}_\lambda(\Delta^N \tilde{\mathbf{x}}) - \Delta^N \tilde{\mathbf{x}}$.
- 3: $\mathbf{s}_0 \leftarrow \Delta^N \boldsymbol{\epsilon}_x$.
- 4: **for** $p = 0 : N - 2$ **do**
- 5: $\mathbf{s}_{p+1} \leftarrow \nabla \mathbf{s}_p \triangleright \nabla$ is the inverse-difference operator defined in (11).
- 6: $\mathbf{s}_{p+1} \leftarrow 2\lambda \left\lceil \frac{\mathbf{s}_{p+1}/\lambda}{2} \right\rceil \triangleright$ rounding to $2\lambda\mathbb{Z}$.
- 7: $\kappa_p \leftarrow \left\lceil \frac{(\nabla^2 \Delta^p \boldsymbol{\epsilon}_x)_1 - (\nabla^2 \Delta^p \boldsymbol{\epsilon}_x)_{J+1}}{12\beta_x} + \frac{1}{2} \right\rceil \triangleright J = \frac{6\beta_x}{\lambda}$.
- 8: $\mathbf{s}_{p+1} \leftarrow \mathbf{s}_{p+1} + 2\lambda\kappa_p$.
- 9: **return** $\bar{\mathbf{x}} \leftarrow \nabla \mathbf{s}_{N-1} + \tilde{\mathbf{x}} + 2a\lambda$, $a \in \mathbb{Z}$.

IV. ONE-BIT SIGNAL RECONSTRUCTION

To reconstruct \mathbf{x} from the sign data $\{\mathbf{r}^{(\ell)}\}_{\ell=1}^m$, we solve the polyhedron search problem through RKA because of its optimal projection and linear convergence in expectation [32, 49, 60].

A. Basic Theory of RKA

The RKA is a *subconjugate gradient method* to solve overdetermined linear systems, i.e., $\mathbf{C}\mathbf{x} \leq \mathbf{b}$ where \mathbf{C} is a $m' \times n'$ matrix with $m' > n'$ [48, 49]. The conjugate-gradient methods turn this inequality to an equality of the following form:

$$(\mathbf{C}\mathbf{x} - \mathbf{b})^+ = 0, \quad (13)$$

and then solve it as any other system of equations. Given a sample index set \mathcal{J} , without loss of generality, rewrite (13) as the polyhedron

$$\begin{cases} \mathbf{c}_j \mathbf{x} \leq b_j & (j \in \mathcal{I}_\leq), \\ \mathbf{c}_j \mathbf{x} = b_j & (j \in \mathcal{I}_=), \end{cases} \quad (14)$$

where $\{\mathbf{c}_j\}$ are the rows of \mathbf{C} and the disjoint index sets \mathcal{I}_\leq and $\mathcal{I}_=$ partition \mathcal{J} . The projection coefficient β_i of the RKA is [49, 60, 61]:

$$\beta_i = \begin{cases} (\mathbf{c}_j \mathbf{x}_i - b_j)^+ & (j \in \mathcal{I}_\leq), \\ \mathbf{c}_j \mathbf{x}_i - b_j & (j \in \mathcal{I}_=). \end{cases} \quad (15)$$

The unknown column vector \mathbf{x} is iteratively updated as

$$\mathbf{x}_{i+1} = \mathbf{x}_i - \frac{\beta_i}{\|\mathbf{c}_j\|_2} \mathbf{c}_j^H, \quad (16)$$

where, at each iteration i , the index j is drawn from the set \mathcal{J} independently at random following the distribution

$$\Pr\{j = k\} = \frac{\|\mathbf{c}_k\|_2^2}{\|\mathbf{C}\|_F^2}. \quad (17)$$

Note that, (7) has only the inequality partition I_{\leq} . Herein, $m' = m \times n$ and $n' = n$. The row vector \mathbf{c}_j and the scalar b_j in the RKA (14)-(17) are j -th row of $-\tilde{\mathbf{\Omega}}$ and j -th element of $-(\text{vec}(\mathbf{R}) \odot \text{vec}(\mathbf{\Gamma}))$, respectively. It may be readily verified that the distribution of choosing a specific sample index j for the inequalities in (7) is uniform, i.e., $\Pr\{j = k\} = \frac{1}{mn}$.

In one-bit reconstruction, $\mathbf{c}_j = -\omega_j$, wherein ω_j is the j -th row of $\tilde{\mathbf{\Omega}}$; a j' -th *coordinate vector* with ± 1 as its j' -th element and

$$j' = \begin{cases} \text{mod}(j, n), & j \neq kn, \\ n, & j = kn, \end{cases} \quad (18)$$

with $1 \leq k \leq m$. This property makes the update process (16) similar to that of the *randomized Gauss-Seidal* method using the coordinate vector in each iteration [49, 62]. This approach is commonly used for solving high-dimensional linear feasibility problems by updating only one dimension at any iteration. The structure of matrix $\tilde{\mathbf{\Omega}}$ leads to a similar efficient RKA implementation by updating only the generic element j' at each iteration, i.e., $(\mathbf{x}_{i+1})_{j'} = (\mathbf{x}_i)_{j'} - \beta_i r_{j'}$, where $r_{j'}$ is the one-bit data at index j' .

B. Error Reconstruction Bound

At the i -th iteration, the error between the RKA estimate \mathbf{x}_i and the optimal solution \mathbf{x}^* has been shown to follow the convergence bound [48, 49, 60, 63]

$$\mathbb{E} \left\{ \|\mathbf{x}_i - \mathbf{x}^*\|_2^2 \right\} \leq q^i \|\mathbf{x}_0 - \mathbf{x}^*\|_2^2, \quad (19)$$

where $q = 1 - \frac{1}{\kappa(\tilde{\mathbf{\Omega}})} \in (0, 1)$ and $\kappa(\tilde{\mathbf{\Omega}}) = \frac{\|\tilde{\mathbf{\Omega}}\|_F^2}{\|\tilde{\mathbf{\Omega}}^\dagger\|_F^2}$ is *scaled condition number* [64] of $\tilde{\mathbf{\Omega}}$, which is a block matrix of m diagonal matrices per (5). We have

$$\|\tilde{\mathbf{\Omega}}\|_F^2 = \sum_{j=1}^{mn} r_j^2 = \sum_{j=1}^{mn} 1 = mn. \quad (20)$$

Moreover, $\|\tilde{\mathbf{\Omega}}^\dagger\|_2^2 = \frac{1}{\sigma_{\min}^2}$, where $\sigma_{\min} = \min\{\sigma_i\}$ is the minimum singular value of $\tilde{\mathbf{\Omega}}$ [65] (maximum singular value is σ_{\max} similarly defined). Following Lemma 1 evaluates singular values of $\tilde{\mathbf{\Omega}}$.

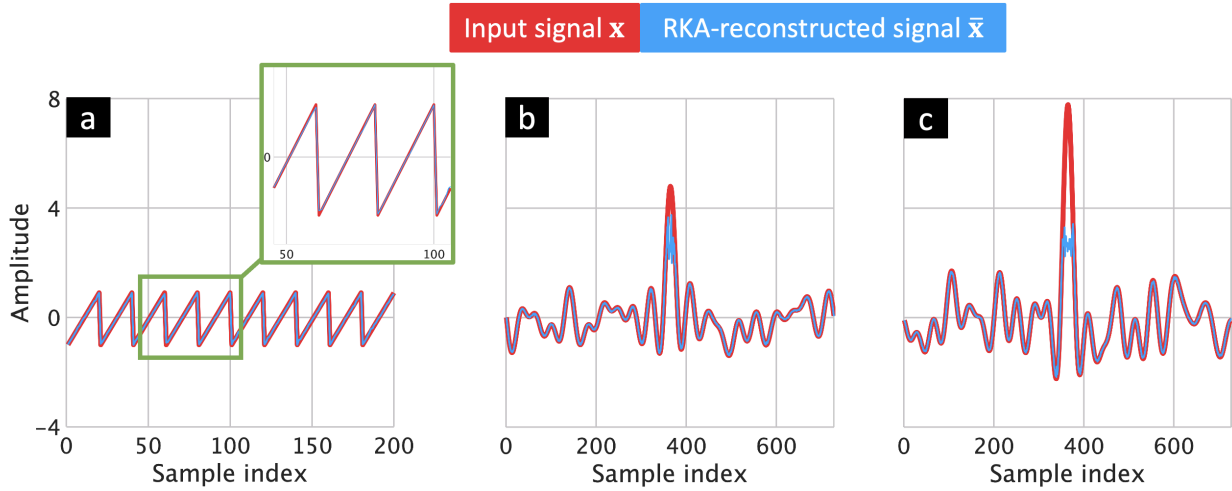


Figure 1. (a) The input sawtooth wave signal \mathbf{x} is reconstructed from one-bit measurements using the RKA to yield $\bar{\mathbf{x}}$. Here, $DR_{\mathbf{x}} = 1$ and $DR_{\tau} = 1$. The inset shows the same plot on a larger scale. (b) As in (a) but for the bandlimited input signal from [18] with $DR_{\mathbf{x}} = 5$. (c) As in (b) but for $DR_{\mathbf{x}} = 8$.

Lemma 1. Consider the concatenation of all m sign data matrices in (5), i.e., $\tilde{\mathbf{\Omega}} \in \mathbb{R}^{mn \times n}$, where n is the size of the input signal and m is the number of time-varying sampling thresholds. The matrix $\tilde{\mathbf{\Omega}}$ is full-rank and its singular values are

$$\sigma_1 = \sigma_2 = \dots = \sigma_n = \sqrt{m}. \quad (21)$$

Proof: Compute the square matrix

$$\begin{aligned} \mathbf{P} &= \tilde{\mathbf{\Omega}}^T \tilde{\mathbf{\Omega}} = \left[\mathbf{\Omega}^{(1)} \mid \dots \mid \mathbf{\Omega}^{(m)} \right] \left[\mathbf{\Omega}^{(1)} \mid \dots \mid \mathbf{\Omega}^{(m)} \right]^T \\ &= \mathbf{\Omega}^{(1)} \left(\mathbf{\Omega}^{(1)} \right)^T + \mathbf{\Omega}^{(2)} \left(\mathbf{\Omega}^{(2)} \right)^T + \dots + \mathbf{\Omega}^{(m)} \left(\mathbf{\Omega}^{(m)} \right)^T, \\ &= m\mathbf{I}. \end{aligned} \quad (22)$$

Hence, the eigenvalues of \mathbf{P} are equal to m . In other words, the singular values of $\tilde{\mathbf{\Omega}}$ are $\{\sigma_i\}_{i=1}^n = \sqrt{m}$. ■

It follows from (20) and Lemma 1 that $\kappa(\tilde{\mathbf{\Omega}}) = \frac{mn}{\sigma_{\min}^2} = n$. Conventionally, the condition number of a matrix is defined as $\frac{\sigma_{\max}}{\sigma_{\min}}$. From Lemma 1, all singular values are equal. Hence, $\kappa(\tilde{\mathbf{\Omega}}) = n \frac{\sigma_{\max}}{\sigma_{\min}}$ is indeed the condition number scaled by n . This leads to

$$q = \frac{n-1}{n}. \quad (23)$$

Set the algorithm termination criterion to the condition

$$\mathbb{E} \left\{ \|\mathbf{x}_i - \mathbf{x}^*\|_2^2 \right\} \leq \epsilon_1, \quad (24)$$

where ϵ_1 is a positive constant. Based on this criterion and (19), the following Proposition 1 states the lower bound on the number of required RKA iterations.

Proposition 1. *The number of RKA iterations i required to achieve the optimal solution \mathbf{x}^* of length n from its one-bit samples within the error specified by (24) is*

$$i \geq \frac{\log\left(\frac{\omega_0}{\epsilon_1}\right)}{\log\left(\frac{1}{1-\frac{1}{n}}\right)}, \quad (25)$$

where $\omega_0 = \|\mathbf{x}_0 - \mathbf{x}^*\|_2^2$ is the initial squared error (at $i = 0$) and ϵ_1 is a positive constant.

Proof: Define $q^i \|\mathbf{x}_0 - \mathbf{x}^*\|_2^2 \leq \epsilon_1$, or equivalently,

$$q^i \leq \frac{\epsilon_1}{\omega_0}. \quad (26)$$

Note that ω_0 is a constant scalar that depends on only the initial and optimal solutions. Substituting (23) in (26) and taking logarithm on both sides yields

$$i \log\left(1 - \frac{1}{n}\right) \leq \log\left(\frac{\epsilon_1}{\omega_0}\right). \quad (27)$$

■

Since the optimal solution is unknown, ω_0 may not be precisely determined. However, a suitable number of required iterations may still be selected following Theorem 1 with a reasonable guess for ω_0 . For instance, an initial value \mathbf{x}_0 may be chosen in the direction of optimal solution \mathbf{x}^* so that a ω_0 is obtained [48, 49].

C. Numerical Example

Fig. 1a illustrates the RKA reconstruction of a sawtooth signal from one-bit polyhedron in (7) for 10 sweeps (periods) with a fundamental frequency of 50 Hz. We discretized the generated signal $x(t)$ at the sampling rate (interval) of 1 kHz ($T = 0.001$ s). The time-varying sampling thresholds were drawn from the distribution $\tau^{(\ell)} \sim \mathcal{N}(\mathbf{0}, \mathbf{I})$, for all $\ell \in \mathcal{L}$. Define the normalized mean squared error, $\text{NMSE} \triangleq \frac{\|\mathbf{x} - \bar{\mathbf{x}}\|_2^2}{\|\mathbf{x}\|_2^2}$, where \mathbf{x} and $\bar{\mathbf{x}}$ denote the true (discretized) signal and its reconstructed version, respectively. Since RKA selects each hyperplane randomly in each iteration, we repeat the reconstruction in Fig. 1a for 15 times. The averaged NMSE over all experiments is only ~ 0.0012 or -29.2082 dB.

D. Limitations of Conventional One-Bit Reconstruction

Denote the DRs of the desired signal \mathbf{x} and the time-varying threshold τ by $\text{DR}_{\mathbf{x}}$ and DR_{τ} , respectively, where we define the DR of a vector as its ℓ_{∞} -norm. *If $\text{DR}_{\mathbf{x}} \leq \text{DR}_{\tau}$, then the reconstructed signal \mathbf{x}^**

may be found inside the polyhedron (7) with a high probability for an adequate number of samples. Otherwise, if $DR_{\mathbf{x}} > DR_{\boldsymbol{\tau}}$, there is no guarantee to obtain \mathbf{x}^* since the desired solution cannot be inside the finite-volume space imposed by the set of inequalities in (7) indicating an irretrievable information loss. We demonstrate this as follows. Without loss of generality, consider $x_k = DR_{\mathbf{x}}$ for $x_k > 0$. Assume $\tau_k^* = \max_{\ell} \tau_k^{(\ell)}$. Since $DR_{\boldsymbol{\tau}} = \|\boldsymbol{\tau}\|_{\infty}$, we have $\tau_k^* \leq DR_{\boldsymbol{\tau}}$. If $DR_{\mathbf{x}} > DR_{\boldsymbol{\tau}}$, then we have $\tau_k^* < DR_{\mathbf{x}} = x_k$. Therefore, to reconstruct the k -th entry of the input signal x_k , we always have a gap $\delta = x_k - \tau_k^* > 0$ that is not covered by any sample to capture the amplitude information of \mathbf{x} . Hence, the desired signal is not found inside the finite-volume space imposed by the inequalities in (7).

In Fig. 1a, $DR_{\boldsymbol{\tau}} = 3$ is larger than $DR_{\mathbf{x}} = 1$ thereby leading to a low reconstruction NMSE. We now consider x to be a bandlimited function with piece-wise constant Fourier transform values are drawn uniformly at random, i.e., $\hat{x}(\omega) \sim \text{unif}(0, 1)$. This signal is the same as the one used in [18]. The time-varying sampling thresholds were generated following the procedure explained in Section IV-C. Fig. 1b shows the RKA-based reconstruction of the bandlimited signal from the polyhedron (7). Around $t = 0$ (corresponding sample index is 364 in the plot), the reconstruction severely degrades because $DR_{\mathbf{x}} = 5$ is set to be larger than $DR_{\boldsymbol{\tau}} = 3$. Indeed, when the difference between $DR_{\mathbf{x}}$ and $DR_{\boldsymbol{\tau}}$ increases further, we observe a significant loss of information in the reconstructed signal (Fig. 1c).

V. TOWARD A RECONSTRUCTION GUARANTEE FOR ONE-BIT SAMPLING

Since RKA does not guarantee an exact signal reconstruction from one-bit measurements in (7) when the DR of the signal exceeds that of the time-varying sampling threshold, it is pertinent to design the time-varying sampling threshold such that $DR_{\mathbf{x}} \leq DR_{\boldsymbol{\tau}}$. This is not always possible because the desired signal is unknown. We address this limitation via UNO, which is our proposed new one-bit sampling method based on the concept of unlimited sampling.

As discussed in Section III, unlimited sampling yields signal amplitudes folded within the range $[-\lambda, \lambda]$. This suggests an alternative time-varying threshold with the same DR as the modulo samples $\tilde{\mathbf{x}} = [\tilde{x}_k]$; i.e. $DR_{\boldsymbol{\tau}} = \lambda$. In other words, the thresholds are modified to be closer to the clipping value and the self-reset ADC is integrated with one-bit sampling. We summarize this UNO sampling framework as follows:

- 1) Apply the modulo operator defined in (8) to the input signal \mathbf{x} and obtain modulo samples $\tilde{\mathbf{x}} = \mathcal{M}_{\lambda}(\mathbf{x})$.
- 2) Design sequences of the time-varying sampling threshold $\{\boldsymbol{\tau}^{(\ell)}\}_{\ell=1}^m$ such that $|DR_{\boldsymbol{\tau}^{(\ell)}} - \lambda| \leq \varepsilon_0$ for all $\ell \in \mathcal{L} = \{1, \dots, m\}$ and a small number ε_0 .
- 3) Apply the one-bit quantization to modulo samples as $\mathbf{r}^{(\ell)} = \text{sgn}(\tilde{\mathbf{x}} - \boldsymbol{\tau}^{(\ell)})$.

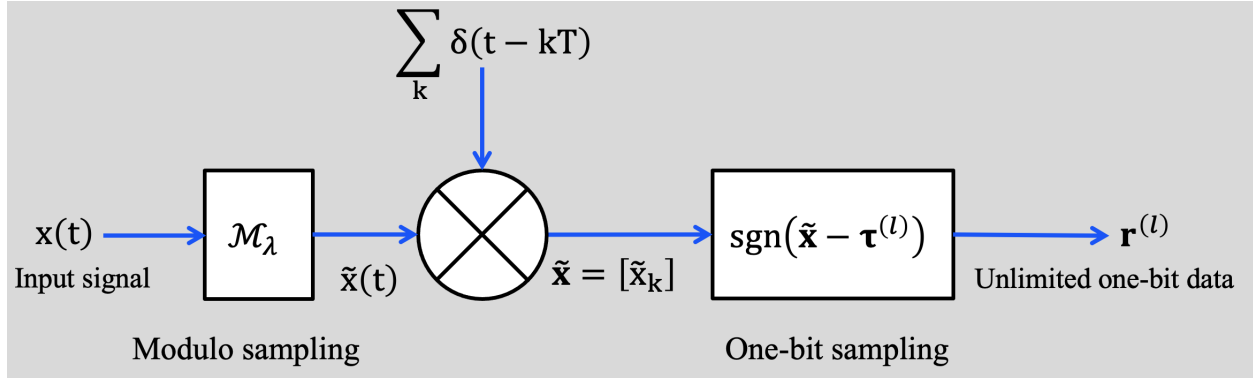


Figure 2. The UNO sampling architecture. The proper choice of the sampling interval T in the middle block is specified by Theorem 2.

Fig. 2 illustrates various steps of our UNO sampling technique. The following Proposition 2 states the UNO threshold design.

Proposition 2 (Judicious threshold design). *Under the UNO sampling framework, the following DR guarantee holds: Assume each one-bit sampling threshold $\tau^{(\ell)}$ is distributed as $\tau^{(\ell)} \sim \mathcal{N}(\mathbf{0}, \sigma_\tau^2 \mathbf{I})$. Then, considering the ADC threshold λ , σ_τ will be equal to $\frac{\lambda}{3}$ with a probability of at least 0.99.*

Proof: With a probability of at least 0.99, the DR of each $\tau^{(\ell)} \sim \mathcal{N}(\mathbf{0}, \sigma_\tau^2 \mathbf{I})$ is $3\sigma_\tau$ [66]. When $\sigma_\tau = \frac{\lambda}{3}$, then time-varying sampling threshold also has a DR of λ with a probability of at least 0.99. ■

In Proposition 2, we design time-varying sampling threshold sequences so that their DR is close to that of the input signal. This enables storing the information of distance between the input signal and the thresholds without any loss of information via one-bit sampling. Fig. 3 shows a comparison of conventional one-bit sampling and UNO for the high DR scenario; the transfer function of the former is plotted in Fig. 3a. We consider the same bandlimited signal as in Section IV-D and a random threshold $\tau \sim \mathcal{N}(\mathbf{0}, \mathbf{I})$. In case of one-bit sampling, the signal values and thresholds differ considerably at some points (Fig. 3b) and, consequently, the information on the distance between the signal value and the threshold samples is completely lost. For UNO, the threshold is chosen closer to the folded signal with $\lambda = 0.5$ (Fig. 3c). This preserves the information of the input signal in the modulo samples (Fig. 3d).

For reconstruction of the signal of interest \mathbf{x} from UNO samples, we reformulate the polyhedron (7) for modulo samples as

$$\tilde{\mathcal{P}} = \left\{ \tilde{\mathbf{x}} \mid \tilde{\mathbf{\Omega}} \tilde{\mathbf{x}} \succeq \text{vec}(\mathbf{R}) \odot \text{vec}(\mathbf{\Gamma}) \right\}. \quad (28)$$

This overdetermined system of linear inequalities in (28) is then solved via RKA and, from the resulting

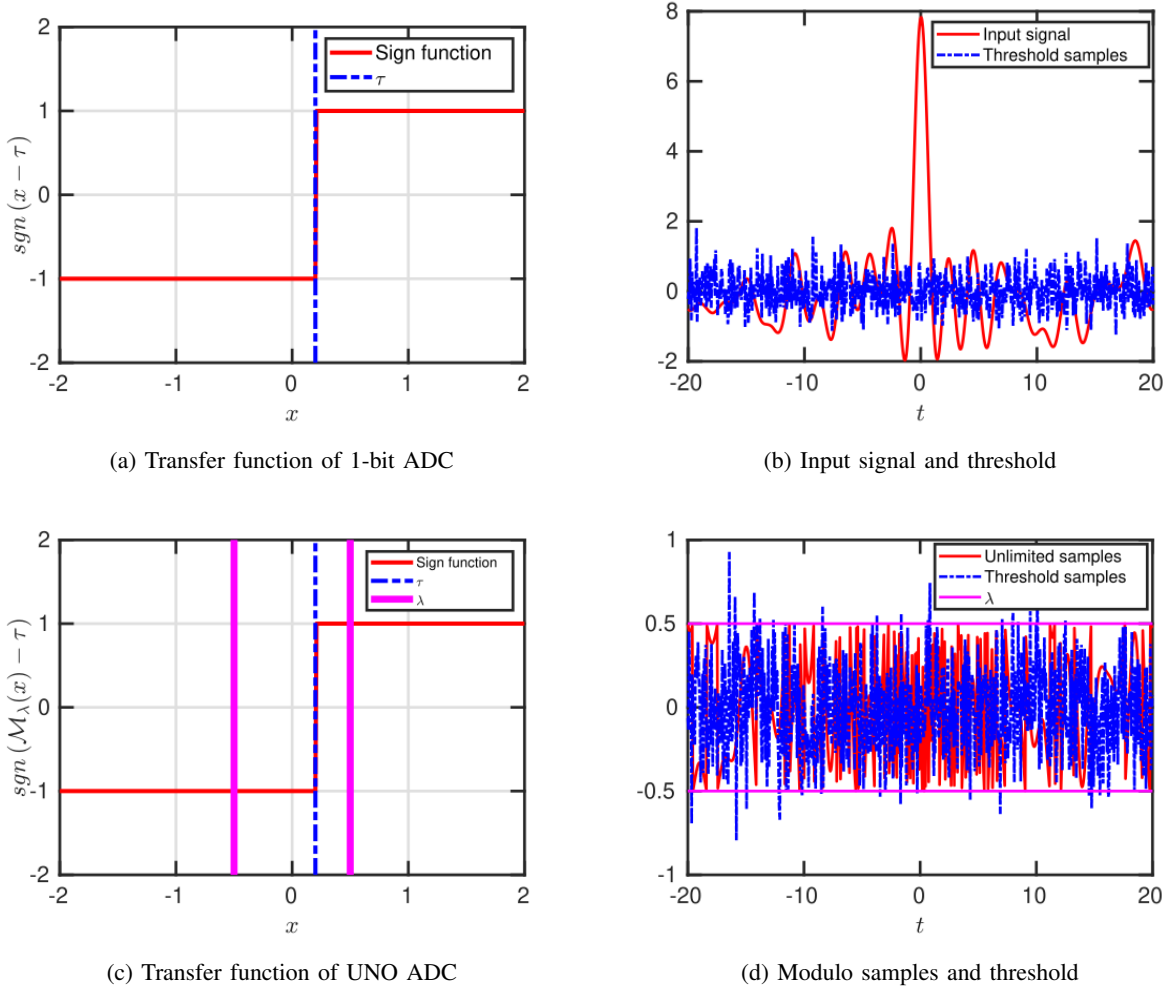


Figure 3. (a) Transfer function of conventional one-bit ADC where the i -th element of the input signal $x = (\mathbf{x})_i$ is compared with a randomly selected threshold τ (b) High DR input signal \mathbf{x} and its threshold samples τ . (c) As in (a), but for UNO with the judicious time-varying threshold λ . (d) The unlimited samples $\tilde{\mathbf{x}}$ compared with the thresholded samples τ and λ .

approximated modulo samples, we obtain \mathbf{x} via Algorithm 1. Algorithm 2 summarizes these steps of the *UNO algorithm*.

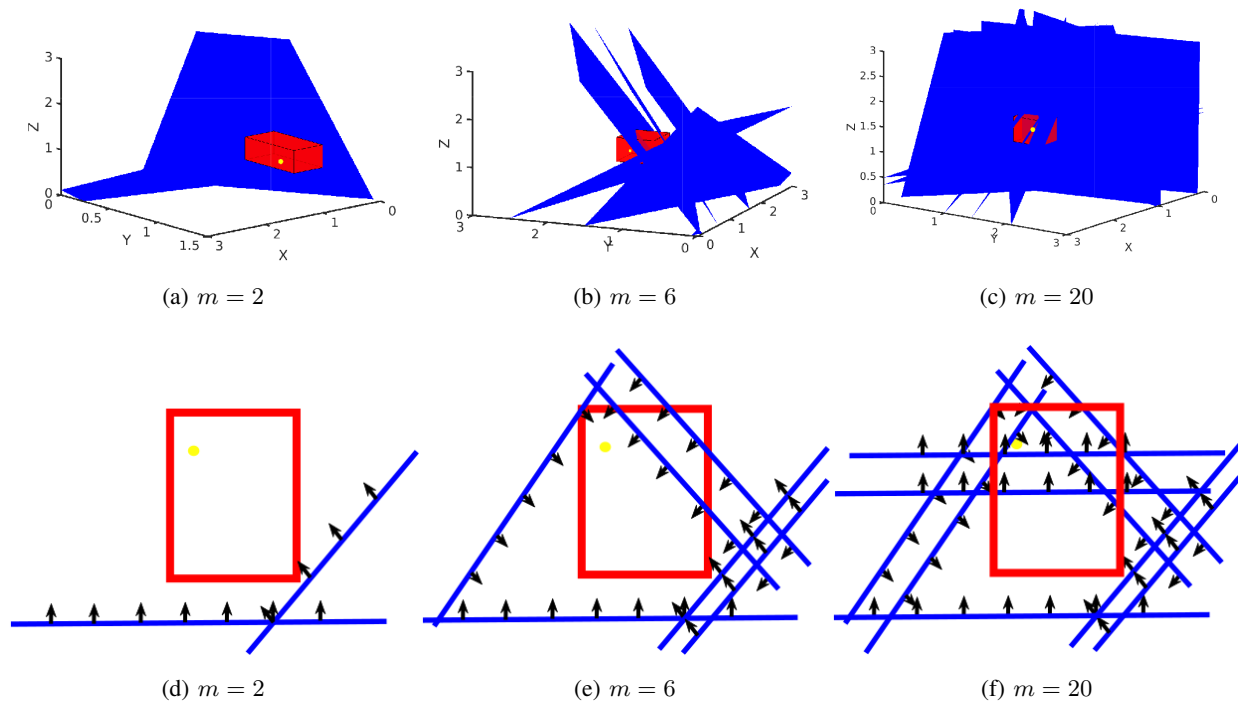


Figure 4. Top: Trihedron space (polyhedron (28) in 3 dimensions) (blue), unlimited sampling cube (red), and true value of the modulo signal $\tilde{\mathbf{x}} \in \mathbb{R}^3$ (yellow) for (a) $m = 2$ (b) $m = 6$ and (c) $m = 20$. Bottom: As in the top panel, but only a cross-section (unshaded with same color boundary) at $Z = 0$ plane is shown for (d) $m = 2$ (e) $m = 6$ and (f) $m = 20$. Each inequality constraint is shown by a half-space whose feasible region is marked by black arrows.

Algorithm 2 Signal reconstruction in UNO.

Input: Sequences of one-bit measurements $\{\mathbf{r}^{(\ell)} = \text{sgn}(\mathcal{M}_\lambda(\mathbf{x}) - \boldsymbol{\tau}^{(\ell)})\}_{\ell=1}^m$, $\boldsymbol{\tau}^{(\ell)} \sim \mathcal{N}(\mathbf{0}, \sigma_\tau^2 \mathbf{I})$,

ADC threshold λ , total number of iterations i_{\max} .

Output: The approximation of the input signal $\bar{\mathbf{x}}$.

- 1: $\mathbf{R} \leftarrow \{\mathbf{r}^{(\ell)}\}_{\ell=1}^m$.
- 2: $\sigma_\tau \leftarrow \frac{\lambda}{3}$
- 3: $\mathbf{\Gamma} \leftarrow \{\boldsymbol{\tau}^{(\ell)}\}_{\ell=1}^m$
- 4: $\boldsymbol{\Omega}^{(\ell)} \leftarrow \text{diag}(\mathbf{r}^{(\ell)})$
- 5: $\tilde{\boldsymbol{\Omega}} \leftarrow \left[\boldsymbol{\Omega}^{(1)} \mid \dots \mid \boldsymbol{\Omega}^{(m)} \right]^\top$
- 6: $\tilde{\mathcal{P}} \leftarrow \left\{ \tilde{\mathbf{x}} \mid \tilde{\boldsymbol{\Omega}} \tilde{\mathbf{x}} \succeq \text{vec}(\mathbf{R}) \odot \text{vec}(\mathbf{\Gamma}) \right\}$.
- 7: Find the modulo signal in $\tilde{\mathcal{P}}$ via RKA.
- 8: **for** $i = 1 : i_{\max}$ **do**
- 9: $\tilde{\mathbf{x}}_{i+1} \leftarrow \tilde{\mathbf{x}}_i + (-\omega_j \tilde{\mathbf{x}}_i + \omega_j \boldsymbol{\tau}^{(\ell)})^+ \omega_j^\top$
- 10: $\bar{\tilde{\mathbf{x}}} \leftarrow \tilde{\mathbf{x}}_{i_{\max}}$
- 11: Reconstruct the input signal via Algorithm 1 from $\bar{\tilde{\mathbf{x}}}$.
- 12: **return** $\bar{\mathbf{x}}$

In Fig. 4, we show that increasing the number m of time-varying sampling threshold sequences guarantees the RKA-based reconstruction as it leads the space formed by the intersection of half-spaces (inequality constraints in (28)) to completely shrink to the true value modulo signal $\tilde{\mathbf{x}}$ inside the volume space imposed by unlimited sampling. This volume space is a *cube* because the constraints applied to the modulo samples are $-\lambda \leq \tilde{x}_k \leq \lambda$. Here, the blue planes/lines representing the linear inequalities form a finite-volume space around the optimal point (displayed by the yellow circle inside the cube) by increasing the number of one-bit sampling thresholds. In the top panel, we show the specific case of a trihedron (i.e., modulo samples are $\tilde{\mathbf{x}} \in \mathbb{R}^3$) to represent the effect of increasing the number of threshold sequences on the reconstruction performance. The bottom panel shows the same effect for 2-D cross-section of the trihedron. The constraints are not enough to create a finite-volume space in Fig. 4a and d. On the other hand, in Fig. 4b and e, such constraints create the desired finite-volume polyhedron space but are unable to capture the optimal point. Finally, in Fig. 4c and f, the optimal point is successfully captured by the resulting finite-volume space. The following theorem summarizes the UNO guarantees.

Theorem 2 (UNO sampling theorem). *Assume $x(t)$ to be a finite energy, bandlimited signal with maximum*

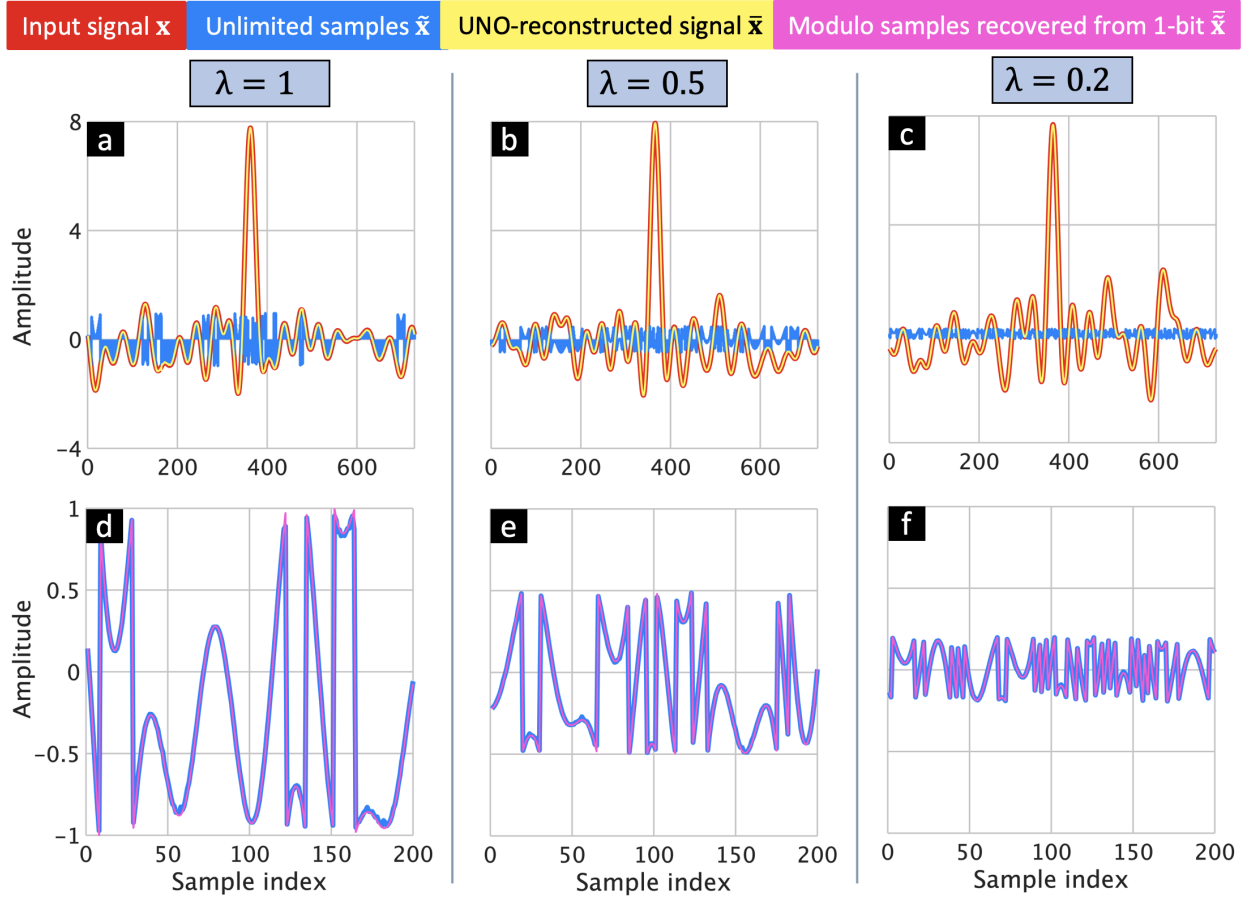


Figure 5. Reconstruction of the input signal from one-bit measurements using UNO when the ADC threshold is (a) $\lambda = 1$, (b) $\lambda = 0.5$, and (c) $\lambda = 0.2$. (d)-(f) As in, respectively, (a)-(c) but the true unlimited samples are compared with their reconstructed samples.

frequency Ω_{max} . Let \tilde{x}_k , $k \in \mathbb{Z}$, introduced in (8) be the modulo samples of $x(t)$ with sampling rate $1/T$. Assume $\bar{\tilde{x}}$ contains the modulo samples reconstructed by the RKA and define the reconstruction error as $\mathbf{e} = (\bar{\tilde{x}} - \tilde{x})$. Then, the sufficient condition for the reconstruction of bandlimited samples x_k from UNO samples $\{\mathbf{r}^{(\ell)} = \text{sgn}(\mathcal{M}_\lambda(\mathbf{x}) - \boldsymbol{\tau}^{(\ell)})\}_{\ell=1}^m$, where $\boldsymbol{\tau}^{(\ell)} \sim \mathcal{N}(\mathbf{0}, \frac{\lambda^2}{9}\mathbf{I})$, up to additive multiples of 2λ is

$$T \leq \frac{1}{2^h \Omega_{max} e}, \quad (29)$$

where $h \in \mathbb{N}$ is given by

$$h \geq \frac{\log\left(\frac{2\beta_x}{\lambda}\right)}{\log\left(\frac{\lambda}{4\|\mathbf{e}\|_\infty}\right)}, \quad (30)$$

and

$$\lambda \geq 4\zeta \|\mathbf{e}\|_\infty, \quad \zeta > 1. \quad (31)$$

Proof: While reconstructing the modulo samples from one-bit data via RKA, the real modulo samples are represented by the linear model

$$\bar{\mathbf{x}} = \tilde{\mathbf{x}} + \mathbf{e}. \quad (32)$$

The error in RKA reconstruction may be viewed as *noise* for modulo samples. According to [43, Theorem 3], the sampling rate for the *contaminated* modulo samples in (32) to reconstruct the bandlimited samples x_k to satisfy $\bar{x}_k = x_k + e_k$ is $T \leq \frac{1}{2^h \Omega_{\max} e}$, where $h \in \mathbb{N}$, and

$$\|\mathbf{e}\|_{\infty} \leq \frac{\lambda}{4} \left(\frac{2\beta_x}{\lambda} \right)^{-\frac{1}{h}}. \quad (33)$$

Clearly, (30) follows from (33). Moreover, to ensure that the log function used in (30) is positive, we have $\frac{\lambda}{4\|\mathbf{e}\|_{\infty}} \geq \zeta > 1$ leading to a lower bound for the ADC threshold $\lambda \geq 4\zeta \|\mathbf{e}\|_{\infty}$. This completes the proof. \blacksquare

Theorem 2 provides the lower bound for the ADC threshold λ in Eq. (31). The upper bound on T for UNO sampling is lower than or equal to that of the unlimited sampling (the equality holds when $h = 1$) which associates with a higher sampling rate in UNO. As mentioned later in Section VI-B, oversampling is a common scenario in one-bit quantization techniques and not a major concern in UNO implementation. Note that the resulting error \mathbf{e} of RKA is different than the noise considered in [43, Theorem 3] in the sense that, unlike the latter, the corresponding reconstructed modulo samples in UNO obey $|\bar{x}_k| < \lambda$. This ensures that N in (12) guarantees $\Delta^N \bar{\mathbf{x}} \equiv \mathcal{M}_{\lambda}(\Delta^N \bar{\mathbf{x}})$ or equivalently $\Delta^N \bar{\mathbf{x}} \equiv \mathcal{M}_{\lambda}(\Delta^N \tilde{\mathbf{x}})$; we refer the reader to [18] for more details on this aspect. As a result, UNO perfectly reconstructs the input samples x_k in the sense that $\bar{x}_k = x_k + e_k$ (up to additive multiples of 2λ) with the same N considered in the noiseless unlimited sampling reconstruction of [43, Section IV.B].

VI. UNO RECONSTRUCTION: NUMERICAL ILLUSTRATIONS AND ERROR ANALYSES

We assessed the performance of the UNO reconstruction through extensive numerical experiments. In particular, we validate that the size of the cube imposed by self-reset ADCs (red contours and shaded regions in Fig. 4) and, hence, the reconstruction error depend on the ADC threshold λ . We then investigate the effect of input signal amplitude $\|\mathbf{x}\|_{\infty}$ on the reconstruction performance. In all experiments, we considered the same high DR input signal as in Section IV-D.

A. Varying ADC Threshold

The number of time-varying sampling thresholds was set to $m = 400$. In each experiment, the generated signals have the same $\text{DR}_{\mathbf{x}} = 8$ but the ADC threshold λ changes. For a given λ , the sequences of time-varying sampling threshold are drawn randomly following the distribution $\left\{ \boldsymbol{\tau}^{(\ell)} \sim \mathcal{N} \left(\mathbf{0}, \frac{\lambda^2}{9} \mathbf{I} \right) \right\}_{\ell=1}^m$.

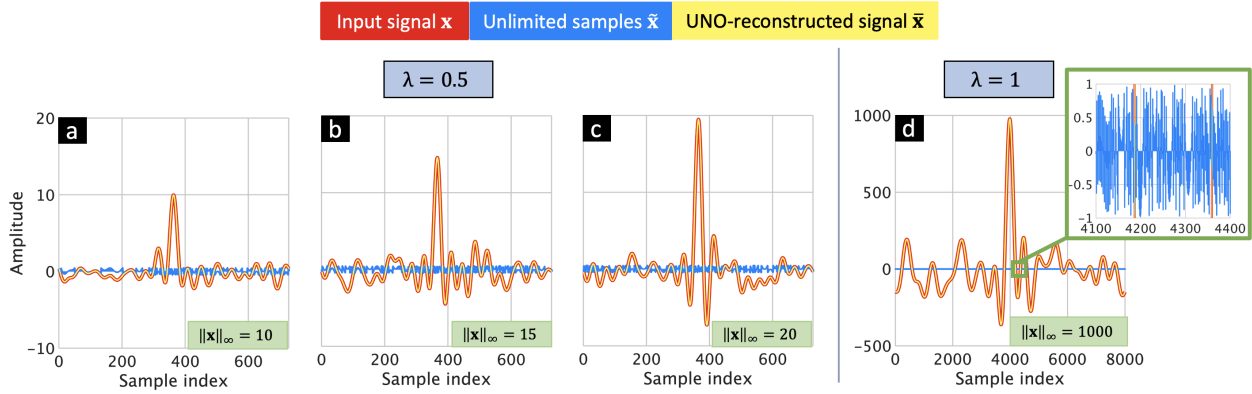


Figure 6. Reconstruction of the input signal from one-bit measurements using UNO Algorithm 2 when the ADC threshold is set to $\lambda = 0.5$ and the input signal amplitude $\|\mathbf{x}\|_\infty$ is (a) 10, (b) 15, and (c) 20. (d) As in (a) but for $\lambda = 1$ and $\|\mathbf{x}\|_\infty = 1000$. The inset shows the same plot on a larger scale.

Fig. 5 illustrates accurate UNO reconstruction for different values of $\lambda \in \{0.2, 0.5, 1\}$. Table I lists the reconstruction NMSE (on a \log_{10} scale), averaged over 15 experiments, for different values of λ . We observe that increasing in λ leads to higher NMSE because the volume of the unlimited sampling cube grows further, and consequently, more hyperplanes may be required to contain a specific volume around the optimal point in the feasible region.

B. Varying Input Signal Amplitude

Here, we generated the input signals with varying DRs. In each experiment, the ADC threshold λ was fixed to $\lambda = 0.5$, for which we generated sequences of time-varying sampling threshold as $\{\boldsymbol{\tau}^{(\ell)} \sim \mathcal{N}(\mathbf{0}, \frac{1}{36}\mathbf{I})\}_{\ell=1}^m$. Fig. 6 shows accurate UNO reconstruction for different values of $\|\mathbf{x}\|_\infty$. Table II reports the corresponding NMSE averaged over 15 experiments.

Next, we study the reconstruction for a signal with an extremely high DR, with $\|x(t)\|_\infty = 1000$. In theory, the unlimited sampling theorem guarantees reconstruction with $T \leq \frac{1}{2\Omega_{\max}e}$. However, in practice, signal reconstruction from unlimited samples has its own limitations due to error propagation by the finite-difference operator. Specifically, for a large DR of input signal compared to that of the ADC threshold λ , the order of difference operator N should also be large. But a large N would also amplify the quantization/round-off noise, leading to an unstable reconstruction. In this scenario, more samples (given by the oversampling factor) are required to decrease N . Note that, unlike conventional ADCs, an abundant number of samples does not lead to an increase in power consumption, manufacturing cost, and per-bit chip area in one-bit ADCs. Fig. 6d shows an accurate UNO reconstruction for $\lambda = 1$ and a 40 times higher sampling rate $1/T$ than the previous experiments.

Table I

AVERAGED UNO RECONSTRUCTION NMSE FOR FIXED \mathbf{x}

λ	0.2	0.5	1
$10 \log_{10} \text{NMSE}$	-72.721	-67.660	-60.987

Table II

AVERAGED UNO RECONSTRUCTION NMSE FOR $\lambda = 0.5$

$\ \mathbf{x}\ _{\infty}$	10	15	20
$10 \log_{10} \text{NMSE}$	-63.925	-65.820	-63.969

Although UNO and one-bit $\Sigma\Delta$ method [51] are different in their respective theoretical foundations and applications, here we compare their reconstruction performance for the same signal. The ADC threshold was set to $\lambda = 1$ and sequences of the time-varying sampling threshold were drawn as $\{\boldsymbol{\tau}^{(\ell)} \sim \mathcal{N}(\mathbf{0}, \frac{1}{9}\mathbf{I})\}_{\ell=1}^m$. For the specific case of $\|\mathbf{x}\|_{\infty} = 40$, Fig. 7 compares the UNO-reconstructed signal $\bar{\mathbf{x}}$ with the one-bit unlimited $\Sigma\Delta$ -reconstructed signal $\bar{\mathbf{x}}_{\Sigma\Delta}$ when the ratio between the input signal amplitude and the ADC threshold $\eta = \frac{\|\mathbf{x}\|_{\infty}}{\lambda}$ is large. The one-bit unlimited $\Sigma\Delta$ degenerates in some parts of the input samples, while the UNO accurately reconstruct the signal. Table III further compares the reconstruction NMSE, averaged over 15 experiments, of both sampling methods for different amplitudes $\|\mathbf{x}\|_{\infty} \in \{20, 50\}$. Here, the degradation in one-bit $\Sigma\Delta$ reconstruction for large η is because of the round-off noise in software and, primarily, imperfect noise shaping in sigma-delta conversion that results in sample corruption.

C. Analysis of Reconstruction Error

To ensure a bounded reconstruction error, the feasible region in (28) cannot have an infinite volume in an asymptotic sense when amplitude constraints are imposed by unlimited sampling. As mentioned before, by introducing more samples, it is possible to obtain a polyhedron with a bounded volume that contains the desired point. Further, as we illustrated in Fig. 4, adding more inequality constraints to (28) leads to shrinkage of this polyhedron. We now prove this result, i.e., in a probabilistic sense, that increasing the number of samples leads to the reconstruction error approaching zero, and that the resulting overdetermined linear system of inequalities guarantees the convergence of RKA [32, 49, 60]. In other words, using an abundant number of samples (or oversampling in one-bit), the probability of creating the finite-volume space around the desired point $\tilde{\mathbf{x}}^*$ is increased.

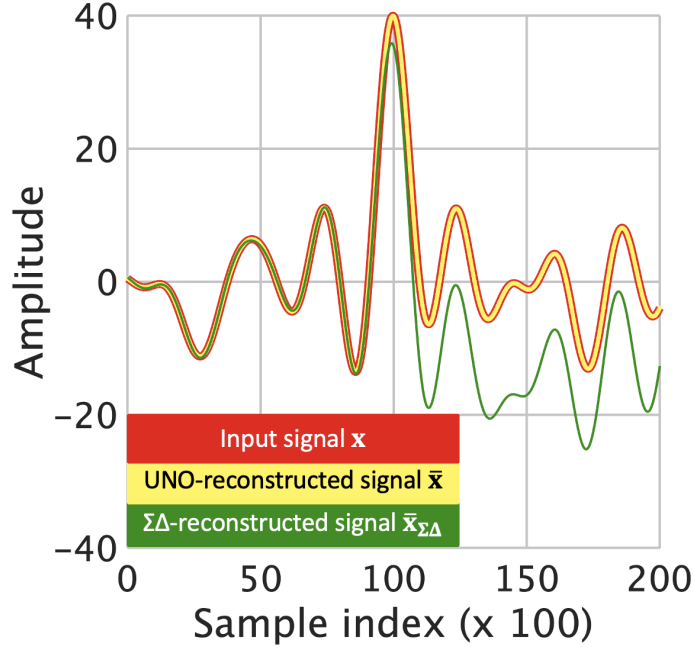


Figure 7. A comparison of reconstruction via UNO and one-bit unlimited $\Sigma\Delta$ when $\lambda = 1$ and $\|\mathbf{x}\|_\infty = 40$.

Table III
RECONSTRUCTION $10 \log_{10}$ NMSE FOR $\lambda = 1$

$\ \mathbf{x}\ _\infty$	One-bit unlimited $\Sigma\Delta$	UNO
20	0.402	-63.969
50	3.777	-62.081

Define the distance between the optimal solution $\tilde{\mathbf{x}}^*$ and the j -th hyperplane of (28) as

$$d_j(\tilde{\mathbf{x}}^*, \boldsymbol{\tau}^{(\ell)}) = \left\| \omega_j (\tilde{\mathbf{x}}^* - \boldsymbol{\tau}^{(\ell)}) \right\|_2^2, \quad j \in \{1, \dots, m'\}, \quad (34)$$

where ω_j is the j -th row of $\tilde{\boldsymbol{\Omega}}$. This distance is also the residual error¹ of (28). Intuitively, it is easy to observe that by reducing the distances between $\tilde{\mathbf{x}}^*$ and the constraint-associated hyperplanes generally increases the possibility of capturing the optimal point. For a specific sample size $m' = mn$, when the volume of the finite space around the optimal point is reduced, the mean $\{d_j(\tilde{\mathbf{x}}^*, \boldsymbol{\tau}^{(\ell)})\}_{j=1}^{m'}$ [49], i.e., $T_{\text{ave}} = \frac{1}{m'} \sum_{j=1}^{m'} d_j(\tilde{\mathbf{x}}^*, \boldsymbol{\tau}^{(\ell)})$, also decreases. Denote $D_\ell(\tilde{\mathbf{x}}^*, \boldsymbol{\tau}^{(\ell)}) = \|\tilde{\mathbf{x}}^* - \boldsymbol{\tau}^{(\ell)}\|_2^2$. Then, T_{ave} becomes

$$T_{\text{ave}} = \frac{1}{m'} \sum_{\ell=1}^m D_\ell(\tilde{\mathbf{x}}^*, \boldsymbol{\tau}^{(\ell)}). \quad (35)$$

¹In a linear feasibility problem $\mathbf{C}\mathbf{x} \leq \mathbf{b}$, the *residual error* is defined as $\|\mathbf{C}\mathbf{x}^* - \mathbf{b}\|_2^2$ [65].

In the one-bit phase retrieval approach studied in [32], a *Chernoff bound* was derived to quantify the possibility of creating the above-mentioned finite-volume and the number of samples required for RKA. We apply this result below in Theorem 3 to the UNO reconstruction from one-bit samples. Here, we have replaced the error between the true value signal and the initial value $\|\tilde{\mathbf{x}}_0 - \tilde{\mathbf{x}}^*\|_2^2$ with the residual error $\|\omega_j(\tilde{\mathbf{x}}^* - \boldsymbol{\tau}^{(\ell)})\|_2^2$ in the Chernoff bound. The latter explains the distance between the hyperplanes and the true value \mathbf{x}^* by including the sampling threshold sequences into its expression.

Theorem 3. [32, Theorem 1] *Assume the distances $\{d_j(\tilde{\mathbf{x}}^*, \boldsymbol{\tau}^{(\ell)})\}_{j=1}^m$ between the desired point $\tilde{\mathbf{x}}^*$ and the hyperplanes of the polyhedron defined in (28) are independent and identically distributed random variables. Then,*

1) *The Chernoff bound of T_{ave} is*

$$\Pr\left(\frac{1}{m'}\sum_{j=1}^{m'}d_j(\tilde{\mathbf{x}}^*, \boldsymbol{\tau}^{(\ell)}) \leq a\right) \geq 1 - \inf_{t \geq 0} \frac{M_T}{e^{ta}}, \quad (36)$$

where a is an average distance point in space at which the finite-volume space around the desired signal is created, and

$$M_T = \left(1 + t \frac{\mu_{d_j}^{(1)}}{m'} + \dots + t^\kappa \frac{\mu_{d_j}^{(\kappa)}}{\kappa! m'^\kappa} + \mathcal{O}(m')\right)^{m'}, \quad (37)$$

is the moment generating function (MGF) of the reconstruction error, $\mu_{d_j}^{(\kappa)} = \mathbb{E}\{d_j^\kappa\}$, and $\mathcal{O}(m')$ denotes the higher-order terms.

2) *M_T decreases with an increase in the sample size leading to an increase in the lower bound in (36).*

Theorem 3 states that the abundant number of samples in conventional one-bit quantization significantly affect the reconstruction performance of RKA for a system of linear inequalities in (28). Based on this result, Claim 1 shows the efficacy of UNO sampling.

Claim 1. *Increasing the number of time-varying sampling threshold sequences m is not an effective approach to guarantee the desired signal reconstruction with RKA without using unlimited sampling.*

Proof: For RKA-based reconstruction in Section IV, assume that we increase the number of time-varying sampling threshold sequences from m to $m + \kappa$. Therefore, from (36) of Theorem 3, the Chernoff bound of the reconstruction error is

$$\Pr\left(\frac{1}{(m + \kappa)n} \sum_{j=1}^{(m + \kappa)n} d_j(\mathbf{x}^*, \boldsymbol{\tau}^{(\ell)}) \leq a\right) \geq 1 - P_T, \quad (38)$$

where $P_T = \inf_{t \geq 0} \frac{M_T}{e^{ta}}$ and $d_j(\mathbf{x}^*, \boldsymbol{\tau}^{(\ell)}) = \|\omega_j(\mathbf{x}^* - \boldsymbol{\tau}^{(\ell)})\|_2^2$. Without loss of generality, assume $x_k = \text{DR}_{\mathbf{x}}$ for $x_k > 0$, and $\delta = x_k - \text{DR}_{\boldsymbol{\tau}}$ when $\text{DR}_{\mathbf{x}} > \text{DR}_{\boldsymbol{\tau}}$. The infimum of the distance $\frac{1}{(m+\kappa)n} \sum_{j=1}^{(m+\kappa)n} d_j(\mathbf{x}^*, \boldsymbol{\tau}^{(\ell)})$ in (38) occurs when $\tau_k^{(\ell)} = \text{DR}_{\boldsymbol{\tau}}$ for $\ell \in \{1, \dots, m+\kappa\}$. As a result, this infimum is

$$\begin{aligned} \bar{d} &= \inf \left(\frac{1}{(m+\kappa)n} \sum_{j=1}^{(m+\kappa)n} d_j(\mathbf{x}^*, \boldsymbol{\tau}^{(\ell)}) \right), \\ &= \inf \left(\frac{1}{(m+\kappa)n} \sum_{j=1}^{(m+\kappa)(n-1)} d_j(\mathbf{x}^*, \boldsymbol{\tau}^{(\ell)}) \right) + \frac{(m+\kappa)\delta}{(m+\kappa)n}, \\ &= \inf \left(\frac{1}{(m+\kappa)n} \sum_{j=1}^{(m+\kappa)(n-1)} d_j(\mathbf{x}^*, \boldsymbol{\tau}^{(\ell)}) \right) + \frac{\delta}{n}. \end{aligned} \quad (39)$$

The term $\frac{\delta}{n}$ in (39) does not depend on the number of time-varying sampling thresholds $m+\kappa$. In other words, increasing the value of m does not guarantee the reconstruction of the desired signal in the polyhedron (7) via the RKA. This phenomenon is also observed in connection to P_T . A considerable difference between the signal values and thresholds leads to larger values of $\{d_j(\mathbf{x}^*, \boldsymbol{\tau}^{(\ell)})\}$ thereby increasing the moments $\{\mu_{d_j}^{(\kappa)}\}$ or MGF M_T . Therefore, the dependence of P_T on M_T is unaffected when m is increased. ■

Note that by using the unlimited sampling and imposing amplitude constraints, the considered distances become bounded and T_{ave} (35) is guaranteed to be lower than a small a . Then, the volume of the resulting finite-space will be smaller than that of the cube imposed by unlimited sampling. In Fig. 8, we show that UNO reconstruction NMSE, averaged over 15 experiments, significantly improves with the increase in the number of time-varying threshold sequences m . The ADC threshold was set to $\lambda = 0.5$ and the signal DR was $\|\mathbf{x}\|_{\infty} = 20$.

Remark 1. According to Theorem 3, when the number of time-varying threshold sequences m is increased, the reconstruction error $\mathbf{e} = (\tilde{\mathbf{x}} - \bar{\mathbf{x}})$ and $\|\mathbf{e}\|_{\infty}$ become smaller. We have a smaller lower bound on h defined in (30) and, consequently, a lower sampling rate based on (29). In other words, a larger m yields a smaller UNO oversampling factor. ■

VII. RECONSTRUCTION IN THE PRESENCE OF NOISE

In the presence of noise, one-bit $\Sigma\Delta$ sampling currently lacks similar guarantees. In one-bit noisy models of [47, 67], a linear measurement model with additive Gaussian noise was considered. Then, based on the MLE formulation for Gaussian likelihood function, the input signal is recovered. However, in case of non-Gaussian contamination, the MLE objective is nonconvex and the recovered solution is

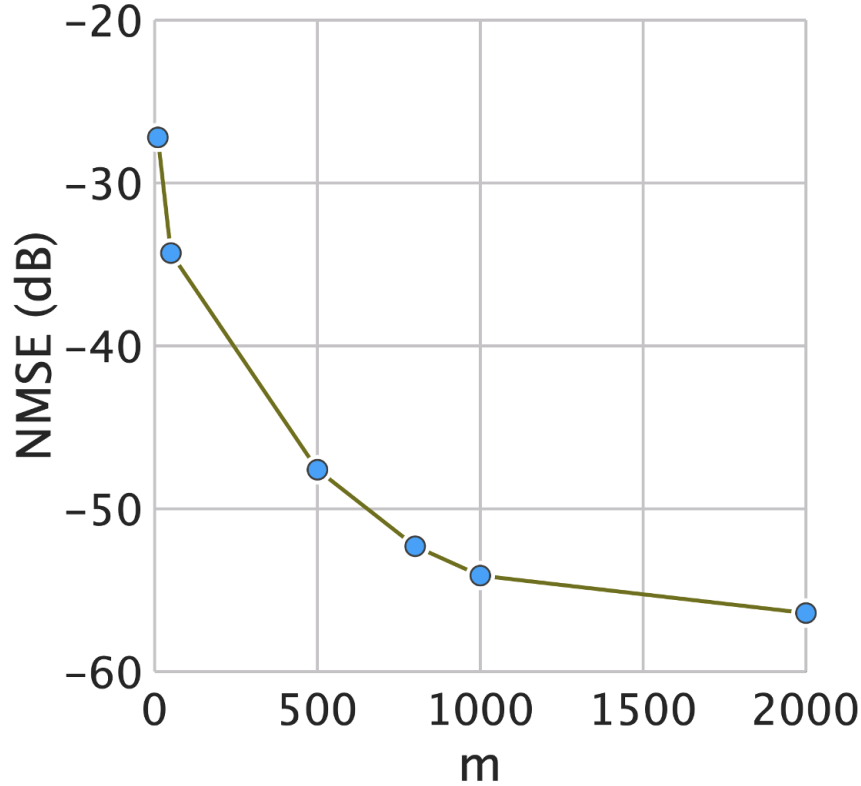


Figure 8. Average NMSE for RKA-based UNO reconstruction with respect to the number of time-varying threshold sequences m for $\lambda = 0.5$ and $\|\mathbf{x}\|_\infty = 20$.

not unique. Moreover, MLE-based reconstruction is computationally more complex for high-dimensional signals.

Previously, for unlimited sampling, [18] has shown recovery of noisy bandlimited samples from their modulo samples up to an unknown additive constant, where the noise is entry-wise additive to the modulo samples, i.e., $\tilde{\mathbf{y}} = \tilde{\mathbf{x}} + \epsilon$, and ϵ is the noise vector. Contrary to this, we propose an approach to reconstruct unlimited one-bit sampled signal when the noise is additive to the input signal, which itself has a linear relationship with a desired parameter. This linear model for the noisy measurement \mathbf{y} is

$$\begin{aligned} \mathbf{y} &= \mathbf{x} + \epsilon, \\ \mathbf{x} &= \mathbf{A}\boldsymbol{\theta}, \quad \mathbf{A} \in \mathbb{R}^{r \times s}, \end{aligned} \tag{40}$$

where $\boldsymbol{\theta}$ is the desired parameter vector and the noise follows the distribution $\epsilon \sim \mathcal{N}(0, \sigma_\epsilon^2 \mathbf{I}_m)$. Here, we may have $\mathbf{y} \notin [-\lambda, \lambda]$. Our goal is to estimate $\boldsymbol{\theta}$ from the UNO samples of noisy measurement \mathbf{y} obtained as

$$\mathbf{r}^{(\ell)} = \text{sgn}(\mathcal{M}_\lambda(\mathbf{y}) - \boldsymbol{\tau}^{(\ell)}), \quad \ell \in \mathcal{L}. \tag{41}$$

Our recovery approach comprises using RKA and Algorithm 1 (with N specified by (55)) to reconstruct noisy measurements from one-bit data, and then exploiting the PnP-ADMM method to estimate the desired parameters from linear overdetermined or undetermined systems.

A. PnP-ADMM-Based UNO Reconstruction

From the UNO samples (41), we reconstruct \mathbf{y} via Algorithm 2. The reconstructed signal $\bar{\mathbf{y}}$ also follows the linear model (40). Therefore, we use $\bar{\mathbf{y}}$ to estimate $\boldsymbol{\theta}$ through the regularization

$$\hat{\boldsymbol{\theta}} = \arg \min_{\boldsymbol{\theta}} \|\bar{\mathbf{y}} - \mathbf{A}\boldsymbol{\theta}\|_2^2 + \eta\rho(\boldsymbol{\theta}), \quad (42)$$

where $\rho(\boldsymbol{\theta})$ is the penalty term and $\eta > 0$ is the real-valued regularization parameter. There is a rich body of literature to select the penalty function $\rho(\cdot)$ including the ℓ_1 -norm [68], smoothly clipped absolute deviation (SCAD) [69], adaptive least absolute shrinkage and selection operator (LASSO) [70] and the minimax-concave (MC) penalty which has a relationship with Huber functions [71].

One of the standard approaches to solve regularized problems such as in (42) is ADMM that relies on splitting variables [72]. We consider

$$\hat{\boldsymbol{\theta}} = \arg \min_{\boldsymbol{\theta}} \|\bar{\mathbf{y}} - \mathbf{A}\boldsymbol{\theta}\|_2^2 + \eta\rho(\boldsymbol{\nu}) \text{ subject to } \boldsymbol{\theta} = \boldsymbol{\nu}. \quad (43)$$

Using the augmented Lagrangian, we reformulate problem (43) as

$$\text{minimize}_{\boldsymbol{\theta}, \boldsymbol{\nu}} \max_{\mathbf{p}} \left\{ \|\bar{\mathbf{y}} - \mathbf{A}\boldsymbol{\theta}\|_2^2 + \eta\rho(\boldsymbol{\nu}) + \mathbf{p}^\top(\boldsymbol{\theta} - \boldsymbol{\nu}) + \frac{\beta}{2}\|\boldsymbol{\theta} - \boldsymbol{\nu}\|^2 \right\}, \quad (44)$$

where \mathbf{p} is the dual variable and β is a real-valued design parameter. Denote $\mathbf{u} = \frac{\mathbf{p}}{\beta}$. Then,

$$\text{minimize}_{\boldsymbol{\theta}, \boldsymbol{\nu}} \max_{\mathbf{u}} \left\{ \|\bar{\mathbf{y}} - \mathbf{A}\boldsymbol{\theta}\|_2^2 + \eta\rho(\boldsymbol{\nu}) + \frac{\beta}{2}\|\boldsymbol{\theta} - \boldsymbol{\nu} + \mathbf{u}\|^2 - \frac{\beta}{2}\|\mathbf{u}\|^2 \right\}. \quad (45)$$

The ADMM tackles (45) by alternating the minimization of $\boldsymbol{\theta}$ and $\boldsymbol{\nu}$. The update of $\boldsymbol{\nu}$ is essentially denoising of $\boldsymbol{\theta}_k + \mathbf{u}_{k-1}$ by the regularization $\eta\rho(\boldsymbol{\nu})$. This is the key idea behind PnP-ADMM, where the proximal projection

$$\boldsymbol{\nu}_k = \arg \min_{\boldsymbol{\nu}} \left\{ \eta\rho(\boldsymbol{\nu}) + \frac{\beta}{2}\|\boldsymbol{\nu} - \boldsymbol{\theta}_k - \mathbf{u}_{k-1}\|^2 \right\} \quad (46)$$

is replaced with an appropriate denoiser $\mathcal{D}(\cdot)$. For further details on various denoisers used in PnP techniques, we refer the interested reader to [52]. Algorithm 3 summarizes the noisy UNO reconstruction procedure.

Algorithm 3 Noisy UNO algorithm.

Input: Sequences of one-bit measurements $\{\mathbf{r}^{(\ell)} = \text{sgn}(\mathcal{M}_\lambda(\mathbf{y}) - \boldsymbol{\tau}^{(\ell)})\}_{\ell=1}^m$, where \mathbf{y} follows (40), $\boldsymbol{\tau}^{(\ell)} \sim \mathcal{N}(\mathbf{0}, \sigma_\tau^2 \mathbf{I})$, ADC threshold λ , design parameters η and β , total number of iterations k_{\max} .

Output: The approximation of the parameter of interest $\hat{\boldsymbol{\theta}}$.

- 1: $\mathbf{R} \leftarrow \{\mathbf{r}^{(\ell)}\}_{\ell=1}^m$.
- 2: $\sigma_\tau \leftarrow \frac{\lambda}{3}$
- 3: $\mathbf{\Gamma} \leftarrow \{\boldsymbol{\tau}^{(\ell)}\}_{\ell=1}^m$
- 4: $\boldsymbol{\Omega}^{(\ell)} \leftarrow \text{diag}(\mathbf{r}^{(\ell)})$
- 5: $\tilde{\boldsymbol{\Omega}} \leftarrow \left[\boldsymbol{\Omega}^{(1)} \mid \dots \mid \boldsymbol{\Omega}^{(m)} \right]^\top$
- 6: $\tilde{\mathcal{P}} \leftarrow \left\{ \tilde{\mathbf{y}} \mid \tilde{\boldsymbol{\Omega}} \tilde{\mathbf{y}} \succeq \text{vec}(\mathbf{R}) \odot \text{vec}(\mathbf{\Gamma}) \right\} \triangleright \tilde{\mathbf{y}}$ reconstructed modulo samples from RKA.
- 7: Reconstruct $\bar{\mathbf{y}}$ from $\tilde{\mathbf{y}}$ with Algorithm 1.
- 8: **for** $k = 1 : k_{\max}$ **do**
- 9: $\boldsymbol{\theta}_k \leftarrow \min_{\boldsymbol{\theta}} \left\{ \|\bar{\mathbf{y}} - \mathbf{A}\boldsymbol{\theta}\|_2^2 + \frac{\beta}{2} \|\boldsymbol{\theta} - \mathbf{v}_{k-1} + \mathbf{u}_{k-1}\|^2 \right\}$.
- 10: $\mathbf{v}_k \leftarrow \mathcal{D}(\boldsymbol{\theta}_k + \mathbf{u}_{k-1})$.
- 11: $\mathbf{u}_k \leftarrow \mathbf{u}_{k-1} + \boldsymbol{\theta}_k - \mathbf{v}_k$.
- 12: **return** $\hat{\boldsymbol{\theta}} \leftarrow \boldsymbol{\theta}_{k_{\max}}$.

B. ADC Threshold Selection in Noisy UNO

Theorem 4 certifies that the additive noise to the input signal results in an additive noise in modulo domain.

Theorem 4. Assume the noise vector in the measurement model $\mathbf{y} = \mathbf{x} + \mathbf{z}$ to be $\mathbf{z} = [z_k] \sim \mathcal{N}(0, \sigma_z^2 \mathbf{I}_m)$.

Denote $\tilde{\mathbf{x}} = \mathcal{M}_\lambda(\mathbf{x})$ and $\tilde{\mathbf{z}} = [\tilde{z}_k]$, $\tilde{z}_k = \text{mod}(z_k, 2\lambda) - 2(1 - q_k)\lambda$, $q_k \in \{0, 1\}$. Then,

$$\tilde{\mathbf{y}} = \tilde{\mathbf{x}} + \tilde{\mathbf{z}}, \quad (47)$$

where $\tilde{\mathbf{y}} = \mathcal{M}_\lambda(\mathbf{y})$.

Proof: Applying the modulo operator \mathcal{M}_λ in (8) to the noisy measurements \mathbf{y} produces

$$\begin{aligned} \tilde{\mathbf{y}} &= \mathcal{M}_\lambda(\mathbf{y}) = \mathcal{M}_\lambda(\mathbf{x} + \mathbf{z}) \\ &= \mathbf{x} + \mathbf{z} - 2\lambda \left\lfloor \frac{\mathbf{x}}{2\lambda} + \frac{1}{2} + \frac{\mathbf{z}}{2\lambda} \right\rfloor, \end{aligned} \quad (48)$$

where $\mathbf{z} \sim \mathcal{N}(0, \sigma_{\mathbf{z}}^2 \mathbf{I}_m)$. Since we have $\lfloor a + b \rfloor \geq \lfloor a \rfloor + \lfloor b \rfloor$ for two arbitrary real numbers a and b , it follows from (48) that

$$\begin{aligned} \mathcal{M}_\lambda(\mathbf{x} + \mathbf{z}) &= \mathbf{x} + \mathbf{z} - 2\lambda \left\lfloor \frac{\mathbf{x}}{2\lambda} + \frac{1}{2} + \frac{\mathbf{z}}{2\lambda} \right\rfloor \\ &\leq \mathbf{x} - 2\lambda \left\lfloor \frac{\mathbf{x}}{2\lambda} + \frac{1}{2} \right\rfloor + \mathbf{z} - 2\lambda \left\lfloor \frac{\mathbf{z}}{2\lambda} \right\rfloor \\ &= \tilde{\mathbf{x}} + \mathbf{z} - 2\lambda \left\lfloor \frac{\mathbf{z}}{2\lambda} \right\rfloor = \tilde{\mathbf{x}} + \text{mod}(\mathbf{z}, 2\lambda). \end{aligned} \quad (49)$$

Using the identity $\lfloor a + b \rfloor \leq \lfloor a \rfloor + \lfloor b \rfloor + 1$, we obtain

$$\mathcal{M}_\lambda(\mathbf{x} + \mathbf{z}) \geq \tilde{\mathbf{x}} + \text{mod}(\mathbf{z}, 2\lambda) - 2\lambda. \quad (50)$$

A binary combination of the right-hand sides of (49) and (50) is equivalent to $\mathcal{M}_\lambda(x_k + z_k)$, i.e.,

$$\begin{aligned} \tilde{y}_k &= \mathcal{M}_\lambda(x_k + z_k) \\ &= q_k (\tilde{x}_k + \text{mod}(z_k, 2\lambda)) + (1 - q_k) (\tilde{x}_k + \text{mod}(z_k, 2\lambda) - 2\lambda), \\ &= \tilde{x}_k + \text{mod}(z_k, 2\lambda) - 2(1 - q_k)\lambda, \end{aligned} \quad (51)$$

where $q_k \in \{0, 1\}$. Rewrite (51) as

$$\tilde{y}_k = \tilde{x}_k + \tilde{z}_k, \quad (52)$$

where $\tilde{z}_k = \text{mod}(z_k, 2\lambda) - 2(1 - q_k)\lambda$, which completes the proof. \blacksquare

It follows from Theorem 4 that the noise corruption in the input signal carries over to the modulo samples. The following theorem unveils the UNO reconstruction guarantee in the presence of noise.

Theorem 5. (*UNO sampling with noise*) Assume $x(t)$ to be a finite energy, bandlimited signal with maximum frequency Ω_{\max} . Let $y(t)$ denote the noisy signal following a linear model $y(t) = x(t) + z(t)$, where $z(t)$ denotes the additive noise signal. Denote the pre-filtered $y(t)$, $x(t)$ and $z(t)$ by, respectively, $y_\phi(t)$, $x_\phi(t)$ and $z_\phi(t)$, where $\phi \in PW_\Omega$ with cut-off frequency Ω_{\max} following a linear model $y_\phi(t) = x_\phi(t) + z_\phi(t)$. Denote the samples of $y_\phi(t)$, $x_\phi(t)$, $z_\phi(t)$ and the modulo samples of $y_\phi(t)$ by, respectively, $(y_\phi)_k$, $(x_\phi)_k$, $(z_\phi)_k$ and $(\tilde{y}_\phi)_k$, where the sampling rate is $1/T$. The modulo samples reconstructed by the RKA are denoted by $\tilde{\mathbf{y}}_\phi$ with the reconstruction error is $\mathbf{e} = (\tilde{\mathbf{y}}_\phi - \tilde{\mathbf{y}}_\phi)$. Then, the sufficient condition to reconstruct bandlimited samples x_k from UNO samples $\{\mathbf{r}^{(\ell)} = \text{sgn}(\mathcal{M}_\lambda(\mathbf{y}_\phi) - \boldsymbol{\tau}^{(\ell)})\}_{\ell=1}^m$, where $\boldsymbol{\tau}^{(\ell)} \sim \mathcal{N}(\mathbf{0}, \frac{\lambda^2}{9} \mathbf{I})$, up to additive multiples of 2λ in the sense that $(\tilde{y}_\phi)_k = x_k + (\tilde{z}_\phi)_k + e_k$ is

$$T \leq \frac{1}{2^h \Omega_{\max} e}, \quad (53)$$

where $(\tilde{z}_\phi)_k$ is defined in Theorem 4 and $h \in \mathbb{N}$ is determined by

$$h \geq \frac{\log\left(\frac{2\beta_x}{\lambda}\right)}{\log\left(\frac{\lambda}{4\|\tilde{\mathbf{z}}_\phi + \mathbf{e}\|_\infty}\right)}, \quad (54)$$

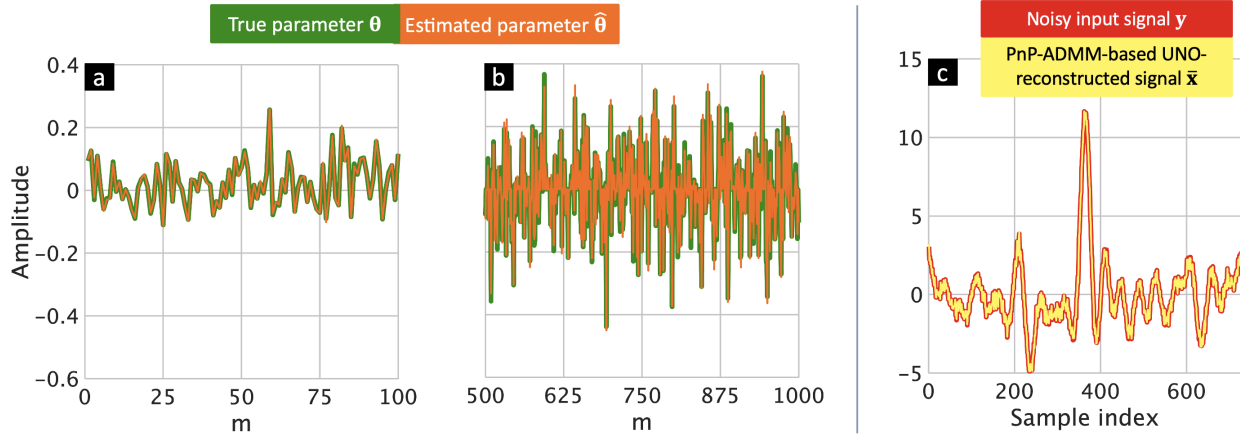


Figure 9. Reconstruction of the desired parameter vector θ following the linear model (40) using PnP-ADMM-based UNO for an (a) overdetermined system with $\mathbf{A} \in \mathbb{R}^{728 \times 100}$ and (b) underdetermined system with $\mathbf{A} \in \mathbb{R}^{728 \times 1000}$. Here, to facilitate a better visual presentation, the number of threshold sequences start from $m = 500$. (c) Reconstruction of the noisy input signal from one-bit measurements using PnP-ADMM-based UNO.

with

$$\lambda \geq 4\zeta \|\tilde{\mathbf{z}}_\phi + \mathbf{e}\|_\infty, \quad \zeta > 1. \quad (55)$$

Proof: The proof, *ceteris paribus*, follows from repeating the proof of Theorem 2 by replacing the RKA error \mathbf{e} with $\tilde{\mathbf{z}}_\phi + \mathbf{e}$. ■

According to Theorem 5, noisy UNO sampling requires more samples (given by the oversampling factor) specified by (53) than the noiseless case in (29). This is similar to other conventional noisy samplers. For example, Cadzow denoising [73], used to suppress the effect of noise in sparse samplers similarly requires such an oversampling [74].

C. Numerical Examples

We investigated PnP-ADMM-based noisy UNO reconstruction with $\mathbf{A} = [a_{ij}]$ to be $a_{ij} \sim \mathcal{N}(0, 1)$ and $\mathbf{y} = \mathbf{y}_t + \boldsymbol{\epsilon}$, where \mathbf{y}_t was generated as in Section IV-D and $\boldsymbol{\epsilon} \sim \mathcal{N}(\mathbf{0}, \sigma_\epsilon^2 \mathbf{I}_m)$. Fig. 9a and b show accurate noisy UNO reconstruction of the parameter vector with fixed $\sigma_\epsilon^2 = 0.1$ in case of, respectively, overdetermined ($r = 728$, $s = 100$) and underdetermined ($r = 728$, $s = 1000$) systems in (40). Fig. 9c demonstrates the efficacy of Noisy UNO in estimating the desired parameter θ from (40) when only UNO samples of noisy measurement \mathbf{y} are available.

Table IV reports the reconstruction NMSE of θ , i.e., $\text{NMSE}_\theta \triangleq \frac{\|\theta - \hat{\theta}\|_2^2}{\|\theta\|_2^2}$, averaged over 15 experiments for different noise variances $\sigma_\epsilon^2 \in \{0.01, 0.05, 0.1\}$ using the PnP-ADMM-based UNO. Here, following

Table IV
RECONSTRUCTION $10 \log_{10} \text{NMSE}_\theta$ WITH PNP-ADMM NOISY UNO

σ_ϵ^2	Overdetermined system	Underdetermined system
0.1	-48.294	-38.128
0.05	-52.676	-42.347
0.01	-56.815	-45.259

Theorem 5, the ADC threshold was set to $\lambda = 1.5$.

VIII. SUMMARY

The design of alternative sampling schemes to enable practical implementations of Shannon’s theorem – from theory to praxis – has been an active research topic for decades. In this context, our proposed UNO presents a framework of merging one-bit quantization and unlimited sampling. This sampling framework naturally facilitates a judicious design of time-varying sampling thresholds by properly utilizing the information on the distance between the signal values and the thresholds in a high DR regime. The noiseless UNO reconstruction relies on exploiting RKA algorithm while the noisy reconstruction is based on the PnP-ADMM heuristic. These low-complexity approaches are preferable over existing costly reconstruction optimization approaches [52, 53].

The UNO framework achieves multiple objectives of high sampling rate, unlimited DR, less complex and potentially low-power implementations. Our numerical and theoretical analyses demonstrate accurate reconstruction for several different scenarios. Some theoretical questions remain open, e.g. on the relationship between the number of threshold sequences m and reconstruction error in a closed form. This may help in finding the required number of thresholds sequences for perfect reconstruction. Further, a hardware verification of UNO on the lines of unlimited sampling in [43] is also desired.

ACKNOWLEDGEMENT

The authors are grateful to Prof. Ayush Bhandari of Imperial College, London for helpful discussions related to his work in [51] and for providing the relevant source codes to facilitate meaningful comparison.

REFERENCES

- [1] A. Cauchy, “Memoire sur diverses formules d’analyse,” *Comptes Rendus de l’Académie des Sciences*, vol. 12, no. 283, pp. 63–78, 1841, in French.
- [2] C.-J. de La Vallée Poussin, “Sur la convergence des formules d’interpolation entre ordonnées equidistantes,” *Bulletins de l’Académie Royale des Sciences, des Lettres et des Beaux Arts de Belgique*, vol. 4, p. 319–403, 1908, in French.

- [3] E. T. Whittaker, "On the functions which are represented by the expansion of interpolating theory," *Proceedings of the Royal Society*, vol. 35, pp. 181–194, 1915.
- [4] K. Ogura, "On a certain transcendental integral function in the theory of interpolation," *Tohoku Mathematical Journal, First Series*, vol. 17, pp. 64–72, 1920.
- [5] V. A. Kotelnikov, "On the transmission capacity of "ether" and wire in electrocommunications," in *Material for the First All-Union Conference on Questions of Communication*, 1933, in Russian.
- [6] H. Raabe, "Untersuchungen an der wechselzeitigen mehrfachübertragung (multiplexübertragung)," Ph.D. dissertation, TH Berlin, 1939, in German.
- [7] C. E. Shannon, "Communication in the presence of noise," *Proceedings of the IRE*, vol. 37, no. 1, pp. 10–21, 1949.
- [8] I. Someya, *Waveform transmission*. Shyukyo Ltd., Tokyo, 1949.
- [9] A. J. Jerri, "The Shannon sampling theorem – Its various extensions and applications: A tutorial review," *Proceedings of the IEEE*, vol. 65, no. 11, pp. 1565–1596, 1977.
- [10] J. A. Hogan and J. D. Lakey, *Duration and bandwidth limiting: Prolate functions, sampling, and applications*. Springer, 2012.
- [11] G. E. Pfander, *Sampling theory, a renaissance: Compressive sensing and other developments*. Springer, 2015.
- [12] T. Kailath, "An application of shannon's rate-distortion theory to analog communication over feedback channels," *Proceedings of the IEEE*, vol. 55, no. 6, pp. 1102–1103, 1967.
- [13] T. Berger, "Rate-distortion theory," in *Wiley Encyclopedia of Telecommunications*, J. G. Proakis, Ed. Wiley Online Library, 2003.
- [14] T. Olofsson, "Deconvolution and model-based restoration of clipped ultrasonic signals," *IEEE Transactions on Instrumentation and Measurement*, vol. 54, no. 3, pp. 1235–1240, 2005.
- [15] A. Adler, V. Emiya, M. G. Jafari, M. Elad, R. Gribonval, and M. Plumbley, "Audio inpainting," *IEEE Transactions on Audio, Speech, and Language Processing*, vol. 20, no. 3, pp. 922–932, 2011.
- [16] J. S. Abel, "Restoring a clipped signal," in *IEEE International Conference On Acoustics, Speech, and Signal Processing*, 1991, pp. 1745–1748.
- [17] S. Ting and A. H. Sayed, "Mitigation of clipping in sensors," in *IEEE International Conference on Acoustics, Speech and Signal Processing*, 2013, pp. 5934–5938.
- [18] A. Bhandari, F. Kraher, and R. Raskar, "On unlimited sampling and reconstruction," *IEEE Transactions on Signal Processing*, vol. 69, pp. 3827–3839, 2020.
- [19] F. Esqueda, S. Bilbao, and V. Välimäki, "Aliasing reduction in clipped signals," *IEEE Transactions on Signal Processing*, vol. 64, no. 20, pp. 5255–5267, 2016.
- [20] V. Gregers-Hansen, S. M. Brockett, and P. E. Cahill, "A stacked A-to-D converter for increased radar signal processor dynamic range," in *IEEE Radar Conference*, 2001, pp. 169–174.
- [21] D. Prasanna, C. R. Murthy, and C. Sriram, "On the application of modulo-ADCs for compressed sensing," in *Asilomar Conference on Signals, Systems, and Computers*, 2021, pp. 852–856.
- [22] A. Bhandari, F. Kraher, and R. Raskar, "On unlimited sampling," in *IEEE International Conference on Sampling Theory and Applications*, 2017, pp. 31–35.
- [23] S. Rudresh, A. Adiga, B. Shenoy, and C. S. Seelamantula, "Wavelet-based reconstruction for unlimited sampling," in *IEEE International Conference on Acoustics, Speech and Signal Processing*, 2018, pp. 4584–4588.
- [24] A. Ameri, J. Li, and M. Soltanalian, "One-bit radar processing and estimation with time-varying sampling thresholds," in *IEEE Sensor Array and Multichannel Signal Processing Workshop*, 2018, pp. 208–212.

- [25] D. K. W. Ho and B. D. Rao, "Antithetic dithered 1-bit massive MIMO architecture: Efficient channel estimation via parameter expansion and PML," *IEEE Transactions on Signal Processing*, vol. 67, no. 9, pp. 2291–2303, 2019.
- [26] T. Kugelstadt, "Active filter design techniques," in *Op Amps for Everyone Literature Number SLOD006A*, R. Mancini, Ed. Texas Instruments, 2002.
- [27] A. Mezghani and A. Swindlehurst, "Blind estimation of sparse broadband massive MIMO channels with ideal and one-bit ADCs," *IEEE Transactions on Signal Processing*, vol. 66, no. 11, pp. 2972–2983, 2018.
- [28] A. Eamaz, F. Yeganegi, and M. Soltanalian, "Modified arcsine law for one-bit sampled stationary signals with time-varying thresholds," in *IEEE International Conference on Acoustics, Speech and Signal Processing*, 2021, pp. 5459–5463.
- [29] S. Sedighi, B. Shankar, M. Soltanalian, and B. Ottersten, "One-bit DoA estimation via sparse linear arrays," in *IEEE International Conference on Acoustics, Speech and Signal Processing*, 2020, pp. 9135–9139.
- [30] C. Qian and J. Li, "ADMM for harmonic retrieval from one-bit sampling with time-varying thresholds," in *IEEE International Conference on Acoustics, Speech and Signal Processing*, 2017, pp. 3699–3703.
- [31] C. Gianelli, L. Xu, J. Li, and P. Stoica, "One-bit compressive sampling with time-varying thresholds for sparse parameter estimation," in *IEEE Sensor Array and Multichannel Signal Processing Workshop*, 2016, pp. 1–5.
- [32] A. Eamaz, F. Yeganegi, and M. Soltanalian, "One-bit phase retrieval: More samples means less complexity?" *IEEE Transactions on Signal Processing*, vol. 70, pp. 4618–4632, 2022.
- [33] A. Eamaz, F. Yeganegi, and M. Soltanalian, "Covariance recovery for one-bit sampled non-stationary signals with time-varying sampling thresholds," *IEEE Transactions on Signal Processing*, 2022.
- [34] P. Wang, J. Li, M. Pajovic, P. T. Boufounos, and P. V. Orlik, "On angular-domain channel estimation for one-bit massive MIMO systems with fixed and time-varying thresholds," in *Asilomar Conference on Signals, Systems, and Computers*, 2017, pp. 1056–1060.
- [35] F. Xi, Y. Xiang, S. Chen, and A. Nehorai, "Gridless parameter estimation for one-bit MIMO radar with time-varying thresholds," *IEEE Transactions on Signal Processing*, vol. 68, pp. 1048–1063, 2020.
- [36] S. Sedighi, K. V. Mishra, M. B. Shankar, and B. Ottersten, "Localization with one-bit passive radars in narrowband internet-of-things using multivariate polynomial optimization," *IEEE Transactions on Signal Processing*, vol. 69, pp. 2525–2540, 2021.
- [37] A. Bhandari, F. Krahmer, and R. Raskar, "Unlimited sampling of sparse signals," in *IEEE International Conference on Acoustics, Speech and Signal Processing*, 2018, pp. 4569–4573.
- [38] F. Ji, P. Pratibha, and W. P. Tay, "On folded graph signals," in *IEEE Global Conference on Signal and Information Processing*, 2019, pp. 1–5.
- [39] S. Fernández-Menduina, F. Krahmer, G. Leus, and A. Bhandari, "DoA estimation via unlimited sensing," in *European Signal Processing Conference*, 2021, pp. 1866–1870.
- [40] A. Bhandari, "Unlimited sampling with sparse outliers: Experiments with impulsive and jump or reset noise," in *IEEE International Conference on Acoustics, Speech and Signal Processing*, 2022, pp. 5403–5407.
- [41] O. Musa, P. Jung, and N. Goertz, "Generalized approximate message passing for unlimited sampling of sparse signals," in *IEEE Global Conference on Signal and Information Processing*, 2018, pp. 336–340.
- [42] D. Florescu and A. Bhandari, "Unlimited sampling with local averages," in *IEEE International Conference on Acoustics, Speech and Signal Processing*, 2022, pp. 5742–5746.
- [43] A. Bhandari, F. Krahmer, and T. Poskitt, "Unlimited sampling from theory to practice: Fourier-Prony recovery and prototype ADC," *IEEE Transactions on Signal Processing*, vol. 70, pp. 1131–1141, 2021.

- [44] M. Beckmann, F. Kraher, and A. Bhandari, "HDR tomography via modulo Radon transform," in *IEEE International Conference on Image Processing*, 2020, pp. 3025–3029.
- [45] D. Florescu, F. Kraher, and A. Bhandari, "Unlimited sampling with hysteresis," in *Asilomar Conference on Signals, Systems, and Computers*, 2021, pp. 831–835.
- [46] S. Khobahi and M. Soltanalian, "Signal recovery from 1-bit quantized noisy samples via adaptive thresholding," in *Asilomar Conference on Signals, Systems, and Computers*, 2018, pp. 1757–1761.
- [47] A. Zymnis, S. Boyd, and E. Candes, "Compressed sensing with quantized measurements," *IEEE Signal Processing Letters*, vol. 17, no. 2, pp. 149–152, 2009.
- [48] T. Strohmer and R. Vershynin, "A randomized Kaczmarz algorithm with exponential convergence," *Journal of Fourier Analysis and Applications*, vol. 15, no. 2, pp. 262–278, 2009.
- [49] D. Leventhal and A. S. Lewis, "Randomized methods for linear constraints: Convergence rates and conditioning," *Mathematics of Operations Research*, vol. 35, no. 3, pp. 641–654, 2010.
- [50] S. Kaczmarz, "Angenäherte auflösung von systemen linearer gleichungen," *Bulletin International de l'Académie Polonaise des Sciences et des Lettres*, vol. 35, p. 355–357, 1937, in German; English translation by Jason Stockmann: "Approximate solution of systems of linear equations".
- [51] O. Graf, A. Bhandari, and F. Kraher, "One-bit unlimited sampling," in *IEEE International Conference on Acoustics, Speech and Signal Processing*, 2019, pp. 5102–5106.
- [52] S. Venkatakrishnan, C. Bouman, and B. Wohlberg, "Plug-and-play priors for model based reconstruction," in *Global Conference on Signal and Information Processing*, 2013, pp. 945–948.
- [53] S. Chan, X. Wang, and O. Elgandy, "Plug-and-Play ADMM for image restoration: Fixed-point convergence and applications," *IEEE Transactions on Computational Imaging*, vol. 3, no. 1, pp. 84–98, 2016.
- [54] S. J. Zahabi, M. M. Naghsh, M. Modarres-Hashemi, and J. Li, "One-bit compressive radar sensing in the presence of clutter," *IEEE Transactions on Aerospace and Electronic Systems*, vol. 56, no. 1, pp. 167–185, 2020.
- [55] K. Knudson, R. Saab, and R. Ward, "One-bit compressive sensing with norm estimation," *IEEE Transactions on Information Theory*, vol. 62, no. 5, pp. 2748–2758, 2016.
- [56] S. Khobahi and M. Soltanalian, "Model-based deep learning for one-bit compressive sensing," *IEEE Transactions on Signal Processing*, vol. 68, pp. 5292–5307, 2020.
- [57] H. Zhu, X. Shang, and J. Li, "Target parameter estimation via one-bit PMCW radar," in *IEEE International Conference on Acoustics, Speech and Signal Processing*, 2020, pp. 9145–9149.
- [58] N. Cassidy and H. Jol, "Ground penetrating radar data processing, modelling and analysis," in *Ground Penetrating Radar: Theory and Applications*, H. M. Jol, Ed. Elsevier Science, 2009, pp. 141–176.
- [59] J. Zhang, J. Hao, X. Zhao, S. Wang, L. Zhao, W. Wang, and Z. Yao, "Restoration of clipped seismic waveforms using projection onto convex sets method," *Scientific Reports*, vol. 6, no. 1, pp. 1–10, 2016.
- [60] J. Briskman and D. Needell, "Block Kaczmarz method with inequalities," *Journal of Mathematical Imaging and Vision*, vol. 52, no. 3, pp. 385–396, 2015.
- [61] L. Dai, M. Soltanalian, and K. Pelckmans, "On the randomized Kaczmarz algorithm," *IEEE Signal Processing Letters*, vol. 21, no. 3, pp. 330–333, 2013.
- [62] A. Ma, D. Needell, and A. Ramdas, "Convergence properties of the randomized extended Gauss–Seidel and Kaczmarz methods," *SIAM Journal on Matrix Analysis and Applications*, vol. 36, no. 4, pp. 1590–1604, 2015.
- [63] B. Polyak, "Gradient methods for solving equations and inequalities," *USSR Computational Mathematics and Mathematical Physics*, vol. 4, no. 6, pp. 17–32, 1964.

- [64] A. Edelman, "On the distribution of a scaled condition number," *Mathematics of computation*, vol. 58, no. 197, pp. 185–190, 1992.
- [65] C. Van Loan and G. Golub, *Matrix computations*. The Johns Hopkins University Press, 1996.
- [66] M. G. Kendall, A. Stuart, and J. Ord, *Kendall's advanced theory of statistics*. Oxford University Press, 1987.
- [67] S. Khobahi and M. Soltanalian, "Model-based deep learning for one-bit compressive sensing," *IEEE Transactions on Signal Processing*, vol. 68, pp. 5292–5307, 2020.
- [68] R. Tibshirani, "Regression shrinkage and selection via the LASSO," *Journal of the Royal Statistical Society: Series B (Methodological)*, vol. 58, no. 1, pp. 267–288, 1996.
- [69] J. Fan and R. Li, "Variable selection via nonconcave penalized likelihood and its oracle properties," *Journal of the American statistical Association*, vol. 96, no. 456, pp. 1348–1360, 2001.
- [70] H. Zou, "The adaptive LASSO and its oracle properties," *Journal of the American statistical association*, vol. 101, no. 476, pp. 1418–1429, 2006.
- [71] I. Selesnick, "Sparse regularization via convex analysis," *IEEE Transactions on Signal Processing*, vol. 65, no. 17, pp. 4481–4494, 2017.
- [72] S. Boyd, N. Parikh, and E. Chu, *Distributed optimization and statistical learning via the alternating direction method of multipliers*. Now Publishers Inc, 2011.
- [73] J. A. Cadzow, "Signal enhancement – A composite property mapping algorithm," *IEEE Transactions on Acoustics, Speech, and Signal Processing*, vol. 36, no. 1, pp. 49–62, 1988.
- [74] S. Rudresh and C. S. Seelamantula, "Finite-rate-of-innovation-sampling-based super-resolution radar imaging," *IEEE Transactions on Signal Processing*, vol. 65, no. 19, pp. 5021–5033, 2017.